Journal of Computational Physics 228 (2009) 8112–8134

Contents lists available at ScienceDirect

Journal of Computational Physics

journal homepage: www.elsevier.com/locate/jcp

Phonon absorbing boundary conditions for molecular dynamics

Murthy N. Guddati *, Senganal Thirunavukkarasu

Department of Civil Engineering, North Carolina State University, Raleigh, NC 27695-7908, USA

ARTICLE INFO

Article history:
Received 13 January 2009
Received in revised form 24 June 2009
Accepted 28 July 2009
Available online 4 August 2009

MSC:
70-08
74S30

PACS:
02.70.Dh
02.70.Ns

Keywords:
Atomistic-to-continuum coupling
Artificial boundary conditions
Absorbing boundary conditions
Perfectly matched layers

ABSTRACT

With the goal of minimizing the domain size for molecular dynamics (MD) simulations, we develop a new class of absorbing boundary conditions (ABCs) that mimic the phonon absorption properties of an unbounded exterior. The proposed MD-ABCs are extensions of perfectly matched discrete layers (PMDLs), originally developed as an absorbing boundary condition for continuous wave propagation problems. Called MD-PMDL, this extension carefully targets the absorption of phonons, the high frequency waves, whose propagation properties are completely different from continuous waves. This paper presents the derivation of MD-PMDL for general lattice systems, followed by explicit application to one-dimensional and two-dimensional square lattice systems. The accuracy of MD-PMDL for phonon absorption is proven by analyzing reflection coefficients, and demonstrated through numerical experiments. Unlike existing MD-ABCs, MD-PMDL is local in both space and time and thus more efficient. Based on their favorable properties, it is concluded that MD-PMDL could provide a more effective alternative to existing MD-ABCs.

1. Introduction

Molecular dynamics (MD) is a widely used method to study physical phenomena at the atomic scale. It offers valuable insights into the behavior of certain macroscopic processes like fracture, which are fundamentally triggered at the atomistic scale. One of the major problems in using MD simulation to study such processes is the computational expense involved in simulating a large system. To make the simulation tractable, the MD domain is usually truncated with simple (Dirichlet/Neumann/Periodic) boundary conditions applied at the truncation boundary. However, a simple boundary condition would result in significant energy being artificially reflected back into the region of interest and can completely distort the physical phenomenon being studied. To minimize this error, the simulation domain is taken to be much larger than the region of interest which significantly increases the computational expense of the simulation. This can be avoided by using a more appropriate boundary condition that mimics the effect of the exterior at the truncation boundary. Applying such a boundary condition leads to a much smaller computational domain, thus resulting in significant savings in computational expense.

The problem discussed above is similar to that of suppressing artificial reflections at the truncation boundary of an infinite domain in continuum wave propagation. This problem has been studied extensively and there exist boundary conditions called absorbing boundary conditions (ABCs) that are quite effective in absorbing the incoming energy thus mimicking the exterior [1,2]. It seems natural to extend these boundary conditions to the discrete domains encountered in MD. However,

* Corresponding author. Tel.: +1 919 515 7699; fax: +1 919 515 7908.
E-mail addresses: murthy.guddati@ncsu.edu (M.N. Guddati), sthirun@ncsu.edu (S. Thirunavukkarasu).

0021-9991/$ - see front matter © 2009 Elsevier Inc. All rights reserved.
doi:10.1016/j.jcp.2009.07.033

since lattice vibrations (phonons) generated in the MD domain have high frequencies and propagate differently from waves in continuous media, continuous ABCs are no longer effective. Instead, ABCs should be derived explicitly for discrete domains to absorb high-frequency phonons. Many ABCs have been developed for this purpose and are summarized in the following paragraphs.

Exact boundary conditions based on the Green's function of the exterior: First developed by Adelman and Doll [3], this approach essentially involves computing the interatomic forces at the truncation boundary through convolution of the boundary response with the exterior Green's function. Cai et al. [4] adopt a similar procedure where the Green's functions for square lattice systems are obtained numerically. Liu and co-workers have extended the idea to more general crystals [5,6]. While these boundary conditions are highly accurate, they are prohibitively expensive and impractical because they involve expensive convolution in time, as well as non-local spatial coupling of boundary atoms.

Rational approximation based methods (rational ABCs): In the context of continuous wave propagation, ABCs are typically derived with the help of rational approximation of the Green's function. These approximations have been directly applied to molecular dynamics simulations [7], but it must be noted that they ignore the discrete dispersion relation and thus cannot accurately absorb high-frequency phonons.

Perfectly matched layer (PML): The PML, also a continuum ABC, involves replacing the exterior with an attenuating medium (PML region) that perfectly matches in impedance with the interior [8], and is truncated using Dirichlet boundary conditions. Due to the impedance matching, there are no reflections at the interface, and due to attenuation in the PML region, the reflection due to truncation is minimal. Owing to its generality and flexibility in applications to complex geometries involving corners, PML is one of the very widely used continuous ABCs, although it has been recently shown that PML may not be as efficient as rational ABCs [9]. PML has been extended to discrete lattice systems in [10], where the interatomic spacing is made complex-valued. This is equivalent to complex stretching in continuous PML that results in wave attenuation (see e.g. [11]). Perfect impedance matching, however, is no longer preserved due to the discrete nature of the problem, leading to significant reflection of high-frequency phonons [12].

Variational boundary condition (VBC): E and co-workers tackle the problem from an optimization view point by using variational principles to minimize the total phonon reflection [13,14]. The basic idea is to increase coupling in the direction normal to the boundary, so as to reduce the extent of coupling in time. The main advantage of VBC is its generality; the procedure is applicable to complex lattice systems. VBC is perhaps the most practical MD-ABC to date in that it is effective in absorbing high-frequency phonons and is more efficient than Green's function based methods. Although the extent of coupling in time is reduced by coupling in space, VBCs still involve convolution operations and are computationally expensive compared to rational ABCs and PMLs. Furthermore, while VBC's stability is ensured through explicit constraints [15], such constraints appear to be sufficient but not necessary for stability, indicating potential degradation of optimal accuracy (for example, the rational ABCs are stable [16] in spite of not satisfying the stability conditions imposed for VBC in [15]). Other minor shortcomings of the method are the lack of transparency in the approximation properties and systematic extension to corners.

In light of the existing ABCs discussed above, it is desirable to obtain a boundary condition that is as accurate as VBCs, as flexible as PMLs (in extension to corners), and as efficient as rational ABCs. To this end, we build on recent research linking continuous PML with rational ABCs [17] to create a class of boundary conditions called perfectly matched discrete layers (PMDLs) [18]. PMDL is essentially PML discretized using linear finite elements with mid-point integration. It has been shown that the integration error exactly cancels the discretization error, thus resulting in perfect matching even after the discretization of the exterior (hence the name, perfectly matched *discrete* layers). Furthermore, PMDL is equivalent to rational ABCs and thus inherits their efficiency while retaining the flexibility of PML. However, PMDL in Refs. [17,18] is developed for continuous wave equation, i.e. PMDL is perfectly matched with the continuous interior, but not with the discrete interior. Thus the continuous PMDL, like other ABCs for wave equation, works well at low frequency limits, but fails in absorbing high frequency phonons. However, we show that the underlying idea of continuous PMDL, namely matching impedance with discrete systems, can be exploited to develop an effective ABC for MD.

Specifically, we show that a PMDL can be viewed as a discrete lattice with nonuniform spacing that has the special property of the characteristic impedance [19] being independent of the atomic spacing. We further show that, for a particular choice of parameters, a PMDL lattice can be made algebraically identical to a general periodic harmonic lattice. Since the PMDL lattice has the additional property of being perfectly matched irrespective of the spacing, any phonon reflections that are introduced due to the truncation of the lattice can be damped out using a few exterior atoms with complex-valued atomic spacing. Named MD-PMDL, the resulting boundary condition is similar in form to continuous PMDL and requires only slightly more computational effort. Compared to existing methods for discrete systems, the proposed method shows promise in providing a more efficient and systematic boundary condition. It should be noted that while MD-PMDL is similar in spirit to continuous PML/PMDL boundary conditions, it is not the same as applying PML/PMDL discretization to the continuum limit equation of the original harmonic lattice. We present both analytical and numerical results that demonstrate this crucial difference.

The outline of the rest of the paper is as follows. The basic problem setup is presented in Section 2 with the help of one-dimensional Frenkel–Kontorova model. Since MD-PMDL is closely related to PMDL, a summary of PMDL ABCs is provided in Section 3, and the extension to a discrete interior is explained in Section 4. The formulation of MD-PMDL including *a-priori* error analysis and a numerical example is presented in Section 5. The extension of MD-PMDL to a square lattice along with numerical examples is presented in Section 6 and the paper is concluded with some closing remarks in Section 7.

2. Preliminaries

We choose the 1-D Frenkel–Kontorova (FK) model to illustrate the ideas in a 1-D setting. A lattice is an infinite chain of atoms with mass m that are spaced apart at a distance h (see Fig. 1(a)). The atoms are labeled with fractional indices, while integer indices are used for the interconnecting cells.

The governing equations for the Frenkel–Kontorova model are given by

$$\begin{aligned} m\ddot{u}_{j+\frac{1}{2}} &= p\left(u_{j+\frac{3}{2}} - 2u_{j+\frac{1}{2}} + u_{j-\frac{1}{2}}\right) - V'_{ext}\left(x_{j+\frac{1}{2}}\right) + f^{ext}_{j+\frac{1}{2}}, \\ x_{j+\frac{1}{2}} &= \left(j+\frac{1}{2}\right)h + u_{j+\frac{1}{2}} \quad \text{for } j = -\infty \cdots \infty, \end{aligned} \tag{1}$$

where u is the displacement field of the atoms, V_{ext} is an external potential field and p describes the strength of nearest-neighbor interaction between the atoms. Let us consider a partition of the 1-D infinite lattice into interior and exterior atoms, corresponding to negative and positive indices, respectively. This results in the partitioning of the cells into three regions (interior, boundary and exterior) as shown in Fig. 1(b). The interior is essentially the region of interest in the MD simulation, while the exterior is to be replaced by an MD-ABC. Specifically, the goal is to devise an MD-ABC at $x_{\frac{1}{2}}$ that mimics the absorption properties of the exterior. It should be emphasized that the dynamics of the exterior is important *only* at the interface as we are merely interested in the propagation of energy from the interior into the exterior.

2.1. Harmonic approximation of the exterior

The potential field is assumed to be a harmonic function in the exterior (this is typical for the development of most MD-ABCs; it appears important to include the entire nonlinear region in the interior). This is a reasonable assumption as the exterior is far away from the region of activity and the displacements of the atoms in the exterior are small. Under this assumption, the force due to the external potential, $V'(x)$, can be approximated by

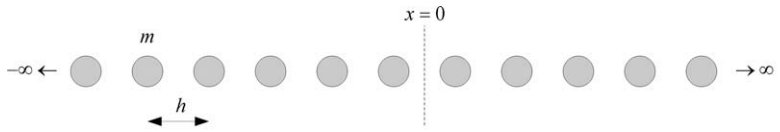

(a) An infinite 1D lattice of atoms with mass m and spacing h.

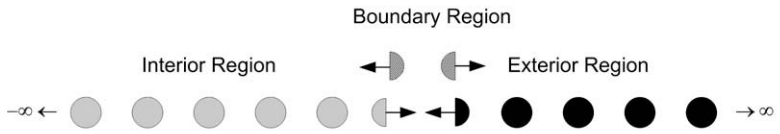

(b) The lattice divided into 3 regions: the **Interior (Gray cells, j < 0)**, the **Boundary(Gray+dashed cell, j = 0)** and the **Exterior (Black cells, j > 0)**.

(c) An expanded view of the Exterior region. The internal force $f_{1/2}$ represents the coupling with the interior.

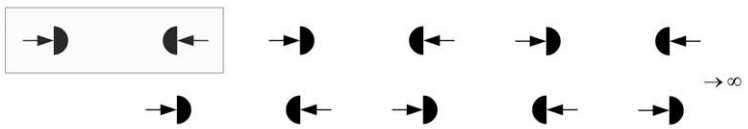

(d) The exterior split into an assembly of two particle systems. The grayed region shows one such system.

Fig. 1. Schematic of an infinite 1-D lattice.

$$V'_{ext}\left(x_{j+\frac{1}{2}}\right) = l u_{j+\frac{1}{2}}, \tag{2}$$

where $l = V''_{ext}\left((j+\frac{1}{2})h\right)$ is the force constant and can be determined by evaluating the linearized force due to the potential about the equilibrium positions. Thus, (1) can be written in frequency domain as

$$-aD^2 u_{j+\frac{1}{2}} - b u_{j+\frac{1}{2}} = f^{ext}_{j+\frac{1}{2}}, \quad j = 0, \ldots, \infty, \tag{3}$$

where $a = ph^2, b = m\omega^2 - l$, and D^2 is the central difference operator given by

$$D^2 u_j = \frac{1}{h^2}(u_{j+1} - 2u_j + u_{j-1}). \tag{4}$$

The reduced Eq. (3) is also known as the discrete wave equation and is used to model the energy transport in a lattice. The propagation of energy in a lattice is usually modeled as the propagation of discrete waves, called phonons, that are governed by the discrete wave equation. Thus, the discrete wave Eq. (3) will be used as the governing equation for the exterior.

2.2. The assembly operator

A lattice is a periodic structure with a unit cell being the basis. Thus, it is natural to express the lattice as an assembly of unit cells as shown in Fig. 1(d). To make the subsequent discussions simpler, the finite element assembly operator [20] is used to represent (3) in a concise form. The assembly operator and the modified equations are discussed next.

Let the equation for an individual unit cell, with index i, be given by

$$\begin{bmatrix} a_i & -b_i \\ -b_i & a_i \end{bmatrix} \mathbf{u_i} = \mathbf{f_i}, \tag{5}$$

where $\mathbf{u}_\mathbf{i}^t = \begin{bmatrix} u_{i-\frac{1}{2}} & u_{i+\frac{1}{2}} \end{bmatrix}$ contains the displacements of the left and right atoms, and $\mathbf{f}_\mathbf{i}^t = \begin{bmatrix} f_{i-\frac{1}{2}} & f_{i+\frac{1}{2}} \end{bmatrix}$ contains the corresponding forces from the rest of the lattice. The assembly operator, $\mathbb{A}$, is defined as

$$\begin{aligned} \left(\mathbb{A}_{i=-\infty}^{\infty} \begin{bmatrix} a & b \\ c & d \end{bmatrix}\right) &= \begin{bmatrix} \ddots & & & \\ & c & a+d & b \\ & & & \ddots \end{bmatrix}, \\ \left(\mathbb{A}_{i=-\infty}^{\infty} \begin{Bmatrix} a \\ b \end{Bmatrix}\right) &= \begin{Bmatrix} \vdots \\ b+a \\ \vdots \end{Bmatrix}, \end{aligned} \tag{6}$$

where i represents the unit cell index. Using the above definitions, the 1-D discrete wave equation can be written as

$$\left(\mathbb{A}_{i=-\infty}^{\infty} \begin{bmatrix} a - \frac{b}{2} & -a \\ -a & a - \frac{b}{2} \end{bmatrix}\right) \mathbf{U} = \mathbf{F}. \tag{7}$$

The assembly operation can also be defined for the case of a 2-D lattice in a similar way. Consider a 2D unit cell given by

$$\mathbf{Au} = \mathbf{f} \equiv \begin{bmatrix} a_{11} & a_{12} & a_{13} & a_{14} \\ a_{21} & a_{22} & a_{23} & a_{24} \\ a_{31} & a_{32} & a_{33} & a_{34} \\ a_{41} & a_{42} & a_{43} & a_{44} \end{bmatrix} \begin{Bmatrix} u_1 \\ u_2 \\ u_3 \\ u_4 \end{Bmatrix} = \begin{Bmatrix} f_1 \\ f_2 \\ f_3 \\ f_4 \end{Bmatrix}, \tag{8}$$

where u_1, u_2, u_3 and u_4 are the displacements at the nodes of the cell. The 2-D assembly can now be concisely expressed as

$$\left(\mathop{\mathbb{A}}_{\substack{i=-\infty,\ldots,\infty \\ j=-\infty,\ldots,\infty}} \{\mathbf{A}\}\right) \mathbf{U} = \left(\mathop{\mathbb{A}}_{\substack{i=-\infty,\ldots,\infty \\ j=-\infty,\ldots,\infty}} \{\mathbf{f}\}\right), \tag{9}$$

where $\underset{\substack{i=-\infty,\ldots,\infty\\ j=-\infty,\ldots,\infty}}{\mathbb{A}}\{\}$ is the 2-D assembly operator defined by

$$\underset{\substack{i=-\infty,\ldots,\infty\\ j=-\infty,\ldots,\infty}}{\mathbb{A}}\{\mathbf{A}\} = \begin{bmatrix} & m_1 & \cdots m_2 & \cdots m_3 & \cdots m_4 & \cdots \\ & \downarrow & \downarrow & \downarrow & \downarrow & \\ m_1 \rightarrow & .. + a_{11} & .. + a_{12} & .. + a_{13} & .. + a_{14} & \\ \vdots & & & & & \\ m_2 \rightarrow & .. + a_{21} & .. + a_{22} & .. + a_{23} & .. + a_{24} & \\ \vdots & & & & & \\ m_3 \rightarrow & .. + a_{31} & .. + a_{32} & .. + a_{33} & .. + a_{34} & \\ \vdots & & & & & \\ m_4 \rightarrow & .. + a_{41} & .. + a_{42} & .. + a_{43} & .. + a_{44} & \\ \vdots & & & & & \end{bmatrix}, \tag{10}$$

$$\underset{\substack{i=-\infty,\ldots,\infty\\ j=-\infty,\ldots,\infty}}{\mathbb{A}}\{\mathbf{f}\} = \begin{Bmatrix} m_1 \rightarrow .. + f_1 \\ \vdots \\ m_2 \rightarrow .. + f_2 \\ \vdots \\ m_3 \rightarrow .. + f_3 \\ \vdots \\ m_4 \rightarrow .. + f_4 \\ \vdots \end{Bmatrix}, \tag{11}$$

where $m_1,\ m_2,\ m_3$ and m_4 are the indices of the displacements u_1, u_2, u_3 and u_4 in the assembled system $\mathbf{U}$.

2.3. Problem statement for a 1-D periodic lattice

For the sake of simplicity, consider a generic harmonic and periodic lattice with the governing equations given by

$$\left(\underset{i=-\infty}{\overset{\infty}{\mathbb{A}}}\begin{bmatrix} p & q \\ r & p \end{bmatrix}\right)\mathbf{U} = \mathbf{F}, \tag{12}$$

where p, q and r depend on the specific governing equation. Let $\mathbf{u_i}, \mathbf{f_i}$ be the displacement, force vectors for the interior, and $\mathbf{u_e}, \mathbf{f_e}$ be the corresponding vectors for the exterior i.e.

$$\mathbf{u_i} = \begin{Bmatrix} u_{-\infty} \\ \vdots \\ u_{-\frac{1}{2}} \end{Bmatrix}, \quad \mathbf{f}_i = \begin{Bmatrix} f_{-\infty} \\ \vdots \\ f_{-\frac{1}{2}} \end{Bmatrix}, \quad \mathbf{u_e} = \begin{Bmatrix} u_{\frac{1}{2}} \\ \vdots \\ u_{\infty} \end{Bmatrix}, \quad \mathbf{f_e} = \begin{Bmatrix} f_{\frac{1}{2}} \\ \vdots \\ f_{\infty} \end{Bmatrix}. \tag{13}$$

The discrete system (13) can now be written as

$$\begin{bmatrix} \mathbf{A_{ii}} & \mathbf{0} \\ \mathbf{0} & \mathbf{A_{ee}} \end{bmatrix}\begin{Bmatrix} \mathbf{u_i} \\ \mathbf{u_e} \end{Bmatrix} = \begin{Bmatrix} \bar{\mathbf{f}}_\mathbf{i} \\ \bar{\mathbf{f}}_\mathbf{e} \end{Bmatrix}, \tag{14}$$

where $\mathbf{A_{ii}}$ and $\mathbf{A_{ee}}$ are given by

$$\begin{aligned} \mathbf{A_{ii}} &= \widehat{\mathbf{P}} + \left(\underset{i=-\infty}{\overset{-1}{\mathbb{A}}}\begin{bmatrix} p & q \\ r & p \end{bmatrix}\right), \quad \widehat{\mathbf{P}} = \begin{bmatrix} \ddots & & \vdots \\ & 0 & 0 \\ \cdots & 0 & p \end{bmatrix}, \\ \mathbf{A_{ee}} &= \overline{\mathbf{P}} + \left(\underset{i=1}{\overset{\infty}{\mathbb{A}}}\begin{bmatrix} p & q \\ r & p \end{bmatrix}\right), \quad \overline{\mathbf{P}} = \begin{bmatrix} p & 0 & \cdots \\ 0 & 0 & \\ \vdots & & \ddots \end{bmatrix}, \end{aligned} \tag{15}$$

and $\bar{\mathbf{f}}_\mathbf{i}$, $\bar{\mathbf{f}}_\mathbf{e}$ are given by

$$\bar{\mathbf{f}}_\mathbf{i} = \mathbf{f}_\mathbf{i} - \begin{Bmatrix} 0 \\ \vdots \\ qu_{\frac{1}{2}} \end{Bmatrix}, \quad \bar{\mathbf{f}}_\mathbf{e} = \mathbf{f}_\mathbf{e} - \begin{Bmatrix} ru_{-\frac{1}{2}} \\ 0 \\ \vdots \end{Bmatrix}. \tag{16}$$

Note that in (16), the interior is coupled to the exterior through the displacement at $i = \frac{1}{2}$ and thus, to solve the interior we only need the displacement at $i = \frac{1}{2}$. Also note that $\bar{\mathbf{f}}_\mathbf{e}$ is zero except at $i = \frac{1}{2}$. Thus, $u_{\frac{3}{2},\frac{5}{2},\ldots,\infty}$ can be eliminated and the effect of the exterior can be written solely in terms of $u_{\frac{1}{2}}$. This is essentially the Dirichlet-to-Neumann (DtN) relation for the exterior and can be written as

$$Ku_{\frac{1}{2}} = f_{\frac{1}{2}}, \tag{17}$$

where K is the DtN map for the exterior. K is also commonly referred to as the discrete half-space stiffness or characteristic impedance [19]; all three terms will be used interchangeably in subsequent discussions. Note that the assumption of zero sources in the exterior implies that the exterior supports only waves traveling to $+\infty$.

Thus, the goal of an MD-ABC can be restated as approximating the DtN map, or the discrete half-space stiffness, of the exterior. This is analogous to the problem of approximating the DtN map of a continuous half-space in continuum wave propagation. This problem has been studied extensively and there exist mature continuous methods that approximate the DtN map in an accurate and efficient manner. We choose a particular class of ABCs called perfectly matched discrete layers (PMDLs) for its generality and flexibility [17,18]. The PMDL boundary conditions are summarized in the next section.

Nonlinear Interactions in the Interior: While the lattice in (13) was considered to be harmonic for simplicity, the above discussion is also valid for a nonlinear lattice. If the interior is nonlinear, A_{ii} in (14) becomes a nonlinear operator and the interior equations are identical to the original problem. The only necessary assumption in the above discussion is that harmonic approximation is valid in the *exterior* region.

3. A summary of perfectly matched discrete layer (PMDL)

3.1. PMDL for the scalar wave equation

PMDL is a class of ABC that approximates the stiffness of a continuous half-space [18]. Though PMDL is applicable to any second-order system [21], for the sake of simplicity the central ideas are summarized using a one-dimensional scalar wave equation. Consider a right half-space with the left boundary at $x = 0$ as shown in Fig. 2(a). Let the governing equation be given by

$$-\frac{\partial^2 u}{\partial x^2} + lu + \frac{\partial^2 u}{\partial t^2} = 0. \tag{18}$$

The reduced form of (18) is

$$-\frac{\partial^2 u}{\partial x^2} - \Lambda u = 0, \tag{19}$$

where $\Lambda = \omega^2 - l$ is a differential operator. Eq. (19) can be decomposed as

$$-\left(\frac{\partial}{\partial x} - \mathrm{i}\sqrt{\Lambda}\right)\left(\frac{\partial}{\partial x} + \mathrm{i}\sqrt{\Lambda}\right)u = 0, \tag{20}$$

where the first factor represents forward propagating waves while the second factor represents backward propagating waves. When the excitation is limited to the boundary, $x = 0$, waves propagate only in the positive x direction. Hence, the governing equation of the right half-space can be written as

$$\frac{\partial u}{\partial x} - ik_x u = 0, \quad k_x = +\sqrt{\Lambda}, \tag{21}$$

where k_x is the wave number. Eq. (21) can be viewed as a relationship between Dirichlet and Neumann data at the boundary $x = 0$. This relation is deceptively simple; note that k_x is the square-root of the differential operator Λ. Due to the irrational nature of the square-root operator, k_x is a pseudo differential operator involving expensive convolution operations. Traditionally, the computational expense is reduced by approximating the square-root operator with a rational function, thus leading to a differential form of (21).

The above procedure of factorization and rational approximation is not possible for all wave equations. PMDL takes a different route and completely circumvents the need for explicit factorization or rational approximation. PMDL derivation, instead involves a multi-step procedure based on complex coordinate stretching and special finite-element discretization of the half-space, that eventually results in a robust approximation of the half-space stiffness leading to an effective one-way wave equation. The steps of the derivation are as follows.

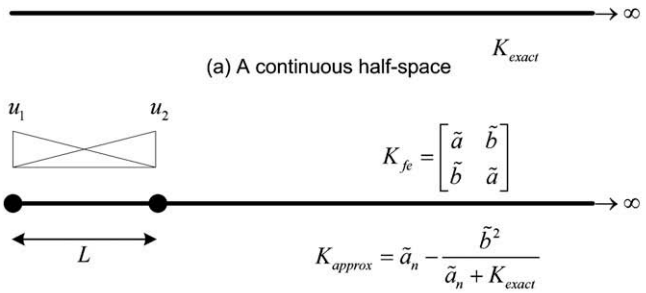

Fig. 2. Steps in the formulation of PMDL.

Step 1. Split the half-space $[0,\infty)$ into a finite element $[0,L]$ and another half-space $[L,\infty)$, with the finite element discretized using linear shape functions as shown in Fig. 2(b). The stiffness matrix of the finite element layer can be easily derived to be

$$K_{fe} = \begin{bmatrix} \tilde{a} & \tilde{b} \\ \tilde{b} & \tilde{a} \end{bmatrix}, \quad \text{where } \begin{matrix} \tilde{a} = \frac{1}{L} - k_x^2 \frac{L}{2}, \\ \tilde{b} = -\frac{1}{L}. \end{matrix} \tag{22}$$

Considering that there is no excitation at the node at $x = L$, the assembled finite-element equations take the form

$$\begin{bmatrix} \tilde{a} & \tilde{b} \\ \tilde{b} & \tilde{a} + K_{exact} \end{bmatrix} \begin{Bmatrix} u_1 \\ u_2 \end{Bmatrix} = \begin{Bmatrix} f_1 \\ 0 \end{Bmatrix}, \tag{23}$$

where K_{exact} is the stiffness of the right half-space, f_1 is the Neumann data at $x = 0$, and u_1, u_2 are the displacements at $x = 0, x = L$, respectively. Eliminating u_2 from (23) results in

$$f_1 = \left(\tilde{a} - \frac{\tilde{b}^2}{\tilde{a} + K_{exact}}\right) u_1. \tag{24}$$

The above equation is a relationship between the Dirichlet and Neumann data of the discretized half-space. The term in the parentheses is effectively the stiffness of the composite half-space. It can be clearly seen that the above relationship is approximate in that, if the exact half-space stiffness is substituted for the right half-space, i.e. $K_{exact} = -ik_x$, the resulting composite half-space stiffness is not recovered (this can be verified easily with the help of (22)).

Step 2 is the key to the development of PMDL and involves the elimination of the finite-element discretization error (with respect to the half-space stiffness at $x = 0$). This is achieved by simply using midpoint integration to approximately evaluate the finite element stiffness matrix resulting in

$$K^{mid\text{-}pt}_{fe\text{-}layer} = \begin{bmatrix} a & b \\ b & a \end{bmatrix}, \quad \text{where} \quad \begin{matrix} a = \frac{1}{L} - k_x^2 \frac{L}{4}, \\ b = -\frac{1}{L} - k_x^2 \frac{L}{4}. \end{matrix} \tag{25}$$

When the above approximation is used, we get the following relationship between the stiffnesses of the composite half-space and the right half-space:

$$K_{composite} = \left(a - \frac{b^2}{a + K_{exact}}\right). \tag{26}$$

It is easy to verify that, when the exact stiffness $(-ik_x)$ is substituted for K_{exact}, we obtain $K_{composite} = -ik_x$, which is also exact (this can be clearly seen by noting that $a^2 - b^2 = K^2_{exact}$). Note that the relationship is exact irrespective of the element length L; it can be arbitrarily large and even complex.

Step 3. The above splitting is recursively applied to discretize the original half-space into an infinite number of finite element layers without introducing any discretization errors. This is equivalent to saying that the assembly

$$\left(\mathop{\mathbb{A}}_{j=1}^{\infty} \left\{ \frac{1}{L_j} \begin{bmatrix} 1 & -1 \\ -1 & 1 \end{bmatrix} - \frac{k_x^2 L_j}{4} \begin{bmatrix} 1 & 1 \\ 1 & 1 \end{bmatrix} \right\}\right), \quad \text{where } L_j = x_j - x_{j-1}, \tag{27}$$

is an exact representation of the the half-space stiffness at $x = 0$.

Step 4. For reasons of computability, the number of layers is limited to n, with a Dirichlet boundary condition applied at $x = x_n$ as shown in Fig. 2(d). However, imposing a Dirichlet boundary condition results in complete reflection of rightward propagating waves and hence this model fails to act as an ABC. This is handled by using the idea that propagating waves are damped out by complex media. By choosing the lengths of the finite element to be complex (see Fig. 2(e)) the incoming energy into the PMDL elements can be damped out and the reflections can be reduced significantly.

3.2. PMDL for a general second-order vector equation

While the arguments in the previous section are explained in the context of scalar wave equation, they are also valid for any second-order vector equation [21]. Specifically, it is shown in [21] that the half-space of a system governed by a second-order vector equation of the form

$$-\mathbf{A}\frac{\partial^2 \mathbf{u}}{\partial x^2} + \mathbf{B}\frac{\partial \mathbf{u}}{\partial x} + \mathbf{C}\mathbf{u} = 0, \tag{28}$$

can be replaced by the infinite assembly

$$\mathop{\mathbb{A}}_{i=1}^{\infty} \left\{ \frac{1}{L_i} \begin{bmatrix} \mathbf{A} & -\mathbf{A} \\ -\mathbf{A} & \mathbf{A} \end{bmatrix} + \frac{1}{2} \begin{bmatrix} -\mathbf{B} & \mathbf{B} \\ -\mathbf{B} & \mathbf{B} \end{bmatrix} + \frac{1}{4} L_i \begin{bmatrix} \mathbf{C} & \mathbf{C} \\ \mathbf{C} & \mathbf{C} \end{bmatrix} \right\} \mathbf{U_e} = \mathbf{F_e}, \tag{29}$$

that preserves the DtN map of the original system at the interface $x = 0$. The assembly operator in (29) can be rewritten as an assembly of Kronecker products, i.e.

$$\mathop{\mathbb{A}}_{i=1}^{\infty} \left\{ \frac{1}{L_i} \begin{bmatrix} 1 & -1 \\ -1 & 1 \end{bmatrix} \otimes \mathbf{A} + \begin{bmatrix} -1 & 1 \\ -1 & 1 \end{bmatrix} \otimes \frac{1}{2}\mathbf{B} + L_i \begin{bmatrix} 1 & 1 \\ 1 & 1 \end{bmatrix} \otimes \frac{1}{4}\mathbf{C} \right\}. \tag{30}$$

If we define basis matrices as

$$\mathbf{A}_{-1} = \begin{bmatrix} 1 & -1 \\ -1 & 1 \end{bmatrix}, \quad \mathbf{A}_0 = \begin{bmatrix} -1 & 1 \\ -1 & 1 \end{bmatrix}, \quad \mathbf{A}_1 = \begin{bmatrix} 1 & 1 \\ 1 & 1 \end{bmatrix}, \tag{31}$$

and coefficient matrices as

$$\mathbf{C}_{-1} = \mathbf{A}, \quad \mathbf{C}_0 = \frac{\mathbf{B}}{2}, \quad \mathbf{C}_1 = \frac{\mathbf{C}}{4}, \tag{32}$$

then (30) can be expressed concisely as

$$\left(\mathop{\mathbb{A}}_{i=1}^{\infty} \left\{ \sum_{f\in\{-1,0,1\}} L_i^f \mathbf{A}_f \otimes \mathbf{C}_f \right\} \right) \mathbf{U_e} = \mathbf{F_e}. \tag{33}$$

4. MD-PMDL: an extension of PMDL for molecular dynamics

In Section 2.3, it was shown that the exterior of a harmonic lattice can be expressed as

$$\left(\overline{\mathbf{P}} + \mathop{\mathbb{A}}_{i=1}^{\infty} \left\{ \begin{bmatrix} p & q \\ r & p \end{bmatrix} \right\} \right) \mathbf{U_e} = \mathbf{F_e}, \tag{34}$$

where $\overline{\mathbf{P}}$ is defined in (15). In fact, for the more generic vector system, the exterior can be written as

$$\left(\overline{\mathbf{P}} + \mathop{\mathbb{A}}_{i=1}^{\infty} \left\{ \begin{bmatrix} \mathbf{P} & \mathbf{Q} \\ \mathbf{R} & \mathbf{P} \end{bmatrix} \right\} \right) \mathbf{U_e} = \mathbf{F_e}, \tag{35}$$

where $\mathbf{P}$, $\mathbf{Q}$ and $\mathbf{R}$ are the stiffness matrices that describe the interaction between the unit cells. Note that (35) can also be expressed as

$$\left(\overline{\mathbf{P}} + \mathop{\mathbb{A}}_{i=1}^{\infty} \left\{ \begin{bmatrix} 1 & -1 \\ -1 & 1 \end{bmatrix} \otimes \mathbf{P}_{-1} + \begin{bmatrix} -1 & 1 \\ -1 & 1 \end{bmatrix} \otimes \mathbf{P}_0 + \begin{bmatrix} 1 & 1 \\ 1 & 1 \end{bmatrix} \otimes \mathbf{P}_1 \right\} \right) \mathbf{U_e} = \mathbf{F_e}, \tag{36}$$

where

$$\mathbf{P}_{-1} = \frac{\mathbf{P}}{2} - \frac{\mathbf{Q}+\mathbf{R}}{4}, \quad \mathbf{P}_0 = \frac{\mathbf{Q}-\mathbf{R}}{2}, \quad \mathbf{P}_1 = \frac{\mathbf{P}}{2} + \frac{\mathbf{Q}+\mathbf{R}}{4}. \tag{37}$$

Using the basis matrices defined in (31, 36) can be concisely written as

$$\left(\overline{\mathbf{P}} + \mathop{\mathbb{A}}_{i=1}^{\infty} \left\{ \sum_{f\in\{-1,0,1\}} \mathbf{A}_f \otimes \mathbf{P}_f \right\} \right) \mathbf{U_e} = \mathbf{F_e}. \tag{38}$$

Note that (38) is identical to the PMDL system in (33) for $L_i = 1$ and $\mathbf{C}_f = \mathbf{P}_f$. Since the stiffness-preserving property of PMDL is independent of L_i, (33) with variable L_i is still an exact representation of the discrete half-space with respect to the stiffness at the interface at $x = 0$. Thus, the discrete half-space can be replaced by PMDL elements such that the characteristic impedance is preserved at every point irrespective of the length of the PMDL elements. However, the PMDL system in (33) is infinite and to make the computation tractable, the system is truncated with a Dirichlet boundary condition applied at the end. This truncation introduces an error in the approximation of the discrete half-space, which can be reduced by choosing complex values for L_i in a manner similar to PMDL. This will be discussed in more detail in Section 5.2, where an error estimate for the boundary condition is derived.

To summarize, the exterior of the discrete lattice in (38) can be approximated in an efficient and accurate manner using the PMDL boundary conditions. The above procedure to extend a continuum ABC to the discrete domain is the central idea of this paper. This particular extension of PMDL to the discrete problem is named MD-PMDL. The details of the formulation of MD-PMDL for 1-D is discussed in subsequent sections.

Remark on crystal symmetry: Due to nonuniform spacing introduced in MD-PMDL, the reader may be concerned with the loss of crystal symmetry. Note that the symmetry is lost only in the exterior; the interior remains unaltered with crystal symmetry completely intact. Since we are interested in the solution in the interior only, the loss of crystal symmetry in the exterior is immaterial. We are only interested in the effect of the exterior on the interior (the DtN map) and this is captured accurately by the PMDL.

Remark on PMDL vs. continuous PML: Note that the reason PMDL could be extended to discrete lattices is that it is perfectly matched with the interior in the discrete sense. Continuous PML, on the other hand, does not preserve perfect matching for discrete systems, i.e. stretching of inter-atomic spacing will alter the characteristic impedance, resulting in spurious reflections at the interface.

5. MD-PMDL formulation for 1-D lattice

Consider the governing equation for the exterior (including boundary cell) in (15):

$$\left(\mathop{\mathbb{A}}_{i=1}^{\infty} \left\{ \begin{bmatrix} p & q \\ r & p \end{bmatrix} \right\} + \overline{\mathbf{P}} \right) \mathbf{U_e} = \mathbf{F_e}. \tag{39}$$

It was shown in the previous sections that the operator on the left can be approximated using a truncated m layered PMDL system, i.e.

$$\mathop{\mathbb{A}}_{i=1}^{\infty}\left\{\begin{bmatrix} p & q \\ r & p \end{bmatrix}\right\}\mathbf{U_e} \approx \mathbb{A}_{i=1}^{m}\left\{\frac{1}{L_i}c_{-1}\mathbf{A}_{-1} + c_0\mathbf{A}_0 + L_i c_1 \mathbf{A}_1\right\}\mathbf{U_e}, \tag{40}$$

where $\mathbf{A}_{-1}, \mathbf{A}_0$ and $\mathbf{A}_1$ are the basis matrices defined in (31) and the coefficients c_{-1}, c_0 and c_1 are given by

$$c_{-1} = \frac{p}{2} - \frac{q+r}{4}, \quad c_0 = \frac{q-r}{2}, \quad c_1 = \frac{p}{2} + \frac{q+r}{4}. \tag{41}$$

Note that $\mathbf{A}_{-1} = \mathbf{v}_{-1}\mathbf{v}_{-1}^t$ and $\mathbf{A}_1 = \mathbf{v}_1\mathbf{v}_1^t$, where $\mathbf{v}_{-1}^t = [-1 \quad 1]$ and $\mathbf{v}_1^t = [1 \quad 1]$. Thus, (40) can be expressed as

$$\left(\mathop{\mathbb{A}}_{i=1}^{m}\left\{\frac{1}{L_i}c_{-1}\mathbf{v}_{-1}\mathbf{v}_{-1}^t + c_0\mathbf{A}_0 + L_i c_1 \mathbf{v}_1\mathbf{v}_1^t\right\} + \overline{\mathbf{P}}\right)\mathbf{U_e} = \mathbf{F_e}. \tag{42}$$

As mentioned in Section 3, the lengths L_i in (42) are chosen to be complex to minimize the error in the approximation. This is discussed in more detail in Section 5.2. Furthermore, the imaginary part of each L_i is made frequency dependent so that the equations are real valued when transformed back into time domain. Hence, the lengths are assumed to be of the form

$$L_i = p_i + \frac{q_i}{iw}, \quad i = 1, \ldots, m, \tag{43}$$

where p_i and q_i are parameters of the method that can be optimized to minimize the error in the approximation. Let us define state variables $s_{1,i}$ and $s_{2,i}$ for a unit cell i as

$$\begin{aligned} s_{1,i} &= \frac{1}{L_i}c_{-1}\mathbf{v}_{-1}^t\mathbf{u}_i, \\ s_{2,i} &= L_i c_1 \mathbf{v}_1^t\mathbf{u}_i. \end{aligned} \tag{44}$$

The governing Eq. (42) can now be expressed in terms of the state variables as

$$\mathop{\mathbb{A}}_{i=1}^{m}\left\{\mathbf{v}_{-1}s_{1,i} + \mathbf{v}_1 s_{2,i}\right\} + \left(\mathbb{A}_{i=1}^{m}\{c_0\mathbf{A}_0\} + \overline{\mathbf{P}}\right)\mathbf{U_e} = \mathbf{F_e}. \tag{45}$$

Since L_i is frequency dependent, $\mathbf{s}_1$ and $\mathbf{s}_2$ are also frequency dependent and can be derived by first substituting (43) into (44) and expanding to get

$$\begin{aligned} p_i(i\omega s_{1,i}) + q_i s_{1,i} &= c_{-1}\mathbf{v}_{-1}^t(i\omega\mathbf{u}_i), \\ (i\omega s_{2,i}) &= c_1\mathbf{v}_1^t(p_i(i\omega\mathbf{u_i}) + q_i\mathbf{u}_i). \end{aligned} \tag{46}$$

The time domain definition of state variables is obtained through an inverse Fourier transform of (46) and is given by

$$\begin{aligned} p_i\frac{\partial s_{1,i}}{\partial t} + q_i s_{1,i} &= c_{-1}\mathbf{v}_{-1}^t\frac{\partial \mathbf{u}_i}{\partial t}, \\ \frac{\partial s_{2,i}}{\partial t} &= c_1\mathbf{v}_1^t\left(p_i\frac{\partial \mathbf{u}_i}{\partial t} + q_i\mathbf{u}_i\right). \end{aligned} \tag{47}$$

Eq. (45) together with (47) is the complete statement of a m-layered MD-PMDL boundary condition for a 1-D lattice and can summarized as

$$\left.\begin{aligned} &\mathop{\mathbb{A}}_{i=1}^{m}\{\mathbf{v}_{-1}s_{1,i} + \mathbf{v}_1 s_{2,i}\} + \left(\mathbb{A}_{i=1}^{m}\{c_0\mathbf{A}_0\} + \overline{\mathbf{P}}\right)\mathbf{U_e} = \mathbf{F_e}, \\ &p_i\frac{\partial s_{1,i}}{\partial t} + q_i s_{1,i} = c_{-1}\mathbf{v}_{-1}^t\frac{\partial \mathbf{u}_i}{\partial t} \\ &\frac{\partial s_{2,i}}{\partial t} = c_1\mathbf{v}_1^t\left(p_i\frac{\partial \mathbf{u}_i}{\partial t} + q_i\mathbf{u}_i\right) \end{aligned}\right\} \quad \text{for } i = 1, \ldots, m. \tag{48}$$

5.1. Time domain implementation

The equations for the exterior at time $t = t_{n+1}$ can be written as

$$\mathop{\mathbb{A}}_{i=1}^{m}\{\mathbf{v}_{-1}s_{1,i}^{n+1} + \mathbf{v}_1 s_{2,i}^{n+1}\} + (\mathbb{A}_{i=1}^{m}\{c_0\mathbf{A}_0\} + \overline{\mathbf{P}})\mathbf{U}_{\mathbf{e}}^{n+1} = \mathbf{F}_{\mathbf{e}}^{n+1}. \tag{49}$$

The state variables s_1^{n+1} and s_2^{n+1} can be obtained by discretizing (47) about $t = t_{n+\frac{1}{2}}$ using the Crank–Nicolson scheme

$$\begin{aligned} \frac{\partial(\cdot)^{n+\frac{1}{2}}}{\partial t} &= \frac{(\cdot)^{n+1} - (\cdot)^n}{\Delta t}, \\ (\cdot)^{n+\frac{1}{2}} &= \frac{(\cdot)^{n+1} + (\cdot)^n}{2}, \end{aligned} \tag{50}$$

to get the following evolution equations for state variables:

$$s_{1,i}^{n+1} = \frac{\hat{r}_i}{r_i} s_{1,i}^n + \frac{c_{-1}}{r_i} \mathbf{v}_{-1}^t \left(\mathbf{u}_i^{n+1} - \mathbf{u}_i^n\right), \tag{51}$$

$$s_{2,i}^{n+1} = s_{2,i}^n + c_1 \mathbf{v}_1^t \left(r_i \mathbf{u}_i^{n+1} - \hat{r}_i \mathbf{u}_i^n\right), \tag{52}$$

where $r_i = p_i + q_i \frac{\Delta t}{2}$ and $\hat{r}_i = p_i - q_i \frac{\Delta t}{2}$. Substituting the expressions for the state variables (51) and (52) into (49), we obtain

$$\begin{aligned} &\mathop{\mathbb{A}}_{i=1}^{m} \left\{ \mathbf{v}_{-1} \frac{\hat{r}_i}{r_i} s_{1,i}^n \right\} + \left(\mathop{\mathbb{A}}_{i=1}^{m} \left\{ \frac{c_{-1}}{r_i} \mathbf{v}_{-1} \mathbf{v}_{-1}^t \right\} \right) (\mathbf{U}_\mathbf{e}^{n+1} - \mathbf{U}_\mathbf{e}^n) + \mathop{\mathbb{A}}_{i=1}^{m} \left\{ \mathbf{v}_1 s_{2,i}^n \right\} + \mathop{\mathbb{A}}_{i=1}^{m} \{ c_1 \mathbf{v}_1 \mathbf{v}_1^t \} \left(r_i \mathbf{U}_\mathbf{e}^{n+1} - \hat{r}_i \mathbf{U}_\mathbf{e}^n \right) \\ &\quad + \left(\overline{\mathbf{P}} + \mathop{\mathbb{A}}_{i=1}^{m} \{ c_0 \mathbf{A}_0 \} \right) \mathbf{U}_\mathbf{e}^{n+1} = \mathbf{F}_\mathbf{e}^{\mathbf{n+1}}. \end{aligned} \tag{53}$$

The above equation can be rearranged and expressed as

$$\mathbf{K_L} \mathbf{U}_\mathbf{e}^{n+1} = \mathbf{F}_\mathbf{e}^{n+1} - \mathbf{F}_\mathbf{sv}^n + \mathbf{K_R} \mathbf{U}_\mathbf{e}^n, \tag{54}$$

where $\mathbf{K_L}$ and $\mathbf{K_R}$ are the stiffness matrices and $\mathbf{F_{sv}}$ is the forcing term due to the state variables and are given by

$$\begin{aligned} \mathbf{K_L} &= \overline{\mathbf{P}} + \mathop{\mathbb{A}}_{i=1}^{m} \left\{ \frac{c_{-1}}{r_i} \mathbf{A}_{-1} + c_0 \mathbf{A}_0 + r_i c_1 \mathbf{A}_1 \right\}, \\ \mathbf{K_R} &= \mathop{\mathbb{A}}_{i=1}^{m} \left\{ \frac{c_{-1}}{r_i} \mathbf{A}_{-1} + \hat{r}_i c_1 \mathbf{A}_1 \right\}, \\ \mathbf{F}_\mathbf{sv}^n &= \mathop{\mathbb{A}}_{i=1}^{m} \left\{ \frac{\hat{r}_i}{r_i} s_{1,i}^n \mathbf{v}_{-1} + s_{2,i}^n \mathbf{v}_1 \right\}. \end{aligned} \tag{55}$$

5.2. Error estimates

Consider a general harmonic and periodic lattice governed by the equation

$$\left(\mathop{\mathbb{A}}_{i=-\infty}^{\infty} \begin{bmatrix} \mathbf{A} & \mathbf{B} \\ \mathbf{C} & \mathbf{A} \end{bmatrix} \right) \mathbf{U} = \mathbf{F}. \tag{56}$$

The solution takes the form $\mathbf{u}_{n+\frac{1}{2}} = \int \bar{\mathbf{u}}(k) e^{ink} \mathrm{d}k$, where each wave mode satisfies the governing Eq. (56). Substituting a single mode, $\bar{\mathbf{u}}(k) e^{ink}$, in (56) results in

$$(\mathbf{C} e^{-ik} + 2\mathbf{A} + \mathbf{B} e^{ik}) \bar{\mathbf{u}}(k) = 0. \tag{57}$$

The relation (57) is more commonly known as the dispersion relation.

The goal here is to find the error in the approximation of the discrete half-space using MD-PMDL layers. Let us consider a wave mode in the interior traveling to the right and incident on the interface. If the exterior is an exact representation of the discrete half-space, then this wave mode would travel into the exterior without causing any reflections at the interface. This is because a half-space can only support outgoing wave modes. However, if the exterior is replaced by MD-PMDL layers, then the inexactness of the exterior would result in waves being reflected into the interior. Thus, the magnitude of the reflected wave compared to the incident wave can be taken as a quantitative measure of the error in the approximation of the discrete half-space.

Consider the solution field in the interior+boundary region $(i \leqslant \frac{1}{2})$:

$$\mathbf{u}_{n+\frac{1}{2}} = \mathbf{I} e^{ink_1} + R\mathbf{I} e^{ink_2} \quad \text{for } n \leqslant 0, \tag{58}$$

where k_1 is the forward propagating wave number, k_2 is the backward propagating wave number, $\mathbf{I}$ is the amplitude of the incident wave mode and $R\mathbf{I}$ is the amplitude of the reflected wave. The scalar R, which is the ratio of the amplitudes of the reflected mode to the incident mode is known as the reflection coefficient. Note that $|R| = 1$ if the wave is completely reflected at the interface and $|R| = 0$ if it is completely absorbed. Thus, a low value of $|R|$ implies a good approximation of the discrete half-space.

The incident and the reflected modes should satisfy the dispersion relation (57), i.e.

$$(\mathbf{C} e^{-ik_1} + 2\mathbf{A} + \mathbf{B} e^{ik_1}) \mathbf{I} = 0, \tag{59}$$

$$R(\mathbf{C} e^{-ik_2} + 2\mathbf{A} + \mathbf{B} e^{ik_2}) \mathbf{I} = 0. \tag{60}$$

Subtracting (59) from (60) and simplifying, we get

$$\begin{aligned} &(e^{k_1} - e^{k_2})(\mathbf{C} e^{-k_1} e^{-k_2} - \mathbf{B}) \mathbf{I} = 0, \\ &\Rightarrow \mathbf{B} e^{k_1} \mathbf{I} = \mathbf{C} e^{-k_2} \mathbf{I} \quad \text{for } k_1 \neq k_2 \end{aligned} \tag{61}$$

Substituting (61) into (59), we get

$$(\mathbf{C}e^{-k_2}+\mathbf{A})\mathbf{I} = -(\mathbf{C}e^{-k_1}+\mathbf{A})\mathbf{I}. \tag{62}$$

Now consider the boundary cell, i.e. $n = 0$. The governing equation for the cell can be written as

$$\begin{bmatrix}\mathbf{A} & \mathbf{B}\\ \mathbf{C} & \mathbf{A}\end{bmatrix}\begin{Bmatrix}\mathbf{u}_{-\frac{1}{2}}\\ \mathbf{u}_{\frac{1}{2}}\end{Bmatrix} = \begin{Bmatrix}\mathbf{f}_{-\frac{1}{2}}\\ \mathbf{f}_{\frac{1}{2}}\end{Bmatrix}. \tag{63}$$

Using the definition of the half-space stiffness (17), i.e. $\mathbf{f}_{\frac{1}{2}} = \mathbf{K}_{\mathbf{approx}}\mathbf{u}_{\frac{1}{2}}$, and substituting (58) into the second equation of (63), we get

$$\begin{aligned}&\mathbf{C}(\mathbf{I}e^{-ik_1}+R\mathbf{I}e^{-ik_2})+\mathbf{A}(\mathbf{I}+R\mathbf{I}) = \mathbf{K}_{\mathbf{approx}}(\mathbf{I}+R\mathbf{I}),\\ &\Rightarrow R(\mathbf{C}e^{-ik_2}+\mathbf{A})\mathbf{I}+(\mathbf{A}+\mathbf{C}e^{-ik_1})\mathbf{I} = \mathbf{K}_{\mathbf{approx}}(1+R)\mathbf{I}.\end{aligned} \tag{64}$$

Note that if the half-space was exact, then $R = 0$ and (64) yields

$$(\mathbf{C}e^{-ik_1}+\mathbf{A})\mathbf{I} = \mathbf{K}_{\mathbf{exact}}\mathbf{I}. \tag{65}$$

Using (62) and (65), (64) can be simplified to

$$\begin{aligned}&(1-R)(\mathbf{C}e^{-k_1}+\mathbf{A})\mathbf{I} = (1+R)\mathbf{K}_{\mathbf{approx}}\mathbf{I}\\ &\Rightarrow (1-R)\mathbf{K}_{\mathbf{exact}}\mathbf{I} = (1+R)\mathbf{K}_{\mathbf{approx}}\mathbf{I}.\end{aligned} \tag{66}$$

Thus, the reflection coefficient R should satisfy the relation

$$\det((1-R)\mathbf{K}_{\mathbf{exact}}-(1+R)\mathbf{K}_{\mathbf{approx}}) = 0. \tag{67}$$

Error estimate for 1-D MD-PMDL: For the 1-D case, reflection coefficient in (67) can be written as

$$R = \frac{K_{exact}-K_{approx}}{K_{exact}+K_{approx}}. \tag{68}$$

Also, the equation of the exterior for the general lattice in (15) is given by

$$\left(\overset{\infty}{\underset{i=1}{\mathbb{A}}}\begin{bmatrix}p & q\\ r & p\end{bmatrix}\right)\mathbf{U} = \mathbf{F}, \tag{69}$$

where p, q and r are scalars. It can be easily shown that the the exact half-space stiffness for the above system is given by $K^2_{exact} = p^2 - qr$.

Assuming n MD-PMDL cells are used in the approximation of the exterior, we have

$$\left(\overset{\infty}{\underset{i=1}{\mathbb{A}}}\begin{bmatrix}p & q\\ r & p\end{bmatrix}\right) \approx \left(\mathbb{A}_{i=1}^{n}\begin{bmatrix}a_i & b_i\\ c_i & a_i\end{bmatrix}\right), \tag{70}$$

where

$$\begin{aligned}a_i &= \frac{1}{2}\left(p-\frac{q+r}{2}\right)\frac{1}{L_i}+\frac{1}{2}\left(p+\frac{q+r}{2}\right)L_i,\\ b_i &= -\frac{1}{2}\left(p-\frac{q+r}{2}\right)\frac{1}{L_i}+\frac{1}{2}(q-r)+\frac{1}{2}\left(p+\frac{q+r}{2}\right)L_i,\\ c_i &= -\frac{1}{2}\left(p-\frac{q+r}{2}\right)\frac{1}{L_i}-\frac{1}{2}(q-r)+\frac{1}{2}\left(p+\frac{q+r}{2}\right)L_i.\end{aligned} \tag{71}$$

If K_n is the stiffness of the n-cell MD-PMDL exterior, then the reflection coefficient is given by

$$R_n = \frac{K_{exact}-K_n}{K_{exact}+K_n}. \tag{72}$$

Note that a_i and b_i have the property

$$a_i^2 - b_i c_i = K^2_{exact}. \tag{73}$$

Also, since PMDL is a rational approximation of the half-space (26), we can write

$$K_i = a_i - \frac{b_i c_i}{a_i + K_{i-1}}. \tag{74}$$

Note that if K_{i-1} is exact, i.e. $K_{i-1} = K_{exact}$, then we recover back the exact half-space stiffness from (74), i.e. $K_i = K_{exact}$. Substituting (74) into (72) and using (73) to simplify, we get the following recursive definition for the reflection coefficient:

$$R_n = \frac{(a_n-K_{exact})(K_{exact}-K_{n-1})}{(a_n+K_{exact})(K_{exact}+K_{n-1})} = \left(\frac{a_n-K_{exact}}{a_n+K_{exact}}\right)R_{n-1}. \tag{75}$$

Since the layers are truncated with a fixed boundary condition we set $K_0 = \infty$. Thus, the magnitude of the reflection coefficient can be written explicitly as

$$|R_n| = \prod_{i=1}^{n} \left| \frac{a_i - K_{exact}}{a_i + K_{exact}} \right|. \tag{76}$$

If K_{exact} is imaginary (propagating modes) and L_i is real, then $|R_n| = 1$ and hence the wave mode will be completely reflected. Thus, to prevent reflection L_i should be imaginary or complex. Similarly, if K_{exact} is real (evanescent wave modes) then L_i has to be real or complex. This is the reason for choosing the general complex form in (43) for the lengths L_i.

Since the aim of MD-PMDL is to be minimize reflections, the lengths L_i should be chosen such that $|R_n|$ is close to 0. Note that since each term is smaller than 1, the product goes to zero exponentially with the number of layers. Thus, the error decays exponentially with the number of MD-PMDL layers. We could optimize the number of layers by choosing optimal values for parameters L_i such that $|R_n|$ is minimized. However, ad hoc values of L_i are used for the simulations in this work and optimization of the parameters is a topic for future study.

A comparison of the error estimates between PMDL and MD-PMDL for the discrete wave equation: Consider the exterior for the 1-D discrete wave Eq. (3) and for simplicity assume $a = h$, $b = hk_x^2$ and $f = 0$, i.e.

$$-D_x^2 u_{j+\frac{1}{2}} - k_x^2 u_{j+\frac{1}{2}} = 0, \quad j = 0, \ldots, \infty \tag{77}$$

or, the equivalent assembly

$$\left(\mathop{\mathbb{A}}_{i=1}^{\infty} \begin{bmatrix} \frac{1}{h} - \frac{k_x^2 h}{2} & -\frac{1}{h} \\ -\frac{1}{h} & \frac{1}{h} - \frac{k_x^2 h}{2} \end{bmatrix} \right) \mathbf{u_e} = \mathbf{f_e}. \tag{78}$$

The MD-PMDL approximation for (78) can be written as

$$\begin{aligned} &\left(\mathbb{A}_{i=1}^{n} \begin{bmatrix} \bar{a}_i & \bar{b}_i \\ \bar{b}_i & \bar{a}_i \end{bmatrix} \right) \mathbf{u_e} = \mathbf{f_e}, \quad \text{where} \\ &\bar{a}_i = \left(\frac{1}{h} - \frac{k_x^2 h}{4} \right) \frac{1}{L_i} - k_x^2 h \frac{L_i}{4} \\ &\bar{b}_i = -\left(\frac{1}{h} - \frac{k_x^2 h}{4} \right) \frac{1}{L_i} - k_x^2 h \frac{L_i}{4}. \end{aligned} \tag{79}$$

Also from (57), the dispersion relation for (78) is given by

$$\begin{aligned} &\frac{1}{h}(e^{-ikh} - 2 + e^{ikh}) = k_x^2 h \\ &\Rightarrow \sin^2 \frac{kh}{2} = \frac{k_x^2 h^2}{4}. \end{aligned} \tag{80}$$

As seen earlier, the discrete half-space stiffness is given by

$$K_{exact}^{disc} = \sqrt{\left(\frac{1}{h} - \frac{k_x^2 h}{2} \right)^2 - \left(\frac{1}{h} \right)^2} = -i \sqrt{k_x^2 \left(1 - \frac{k_x^2 h^2}{4} \right)}. \tag{81}$$

Using (80) and (81) can be simplified to get

$$K_{exact}^{disc} = -\frac{i}{h} \sin(kh). \tag{82}$$

Substituting (82) and (79) in (76), the reflection coefficient becomes

$$\left| R_n^{md\text{-}pmdl} \right| = \prod_{j=1}^{n} \left| \frac{ih - L_j \tan\left(\frac{kh}{2}\right)}{ih + L_j \tan\left(\frac{kh}{2}\right)} \right|^2. \tag{83}$$

The reflection coefficient when PMDL is used for the right exterior is given by

$$R_n^{pmdl} = \frac{K_{exact}^{disc} - K_{pmdl}}{K_{exact}^{disc} + K_{pmdl}}, \tag{84}$$

where K_{pmdl} is the stiffness of the PMDL layers formulated for the system obtained as the continuum limit ($h \to 0$) of the discrete wave equation,

$$-\frac{\partial^2 u}{\partial x^2} - k_x^2 u = f. \tag{85}$$

The reflection coefficient when PMDL is used to approximate the continuous half-space stiffness of (85) is given by

$$R_n^{cont} = \frac{K_{exact}^{cont} - K_{pmdl}}{K_{exact}^{cont} + K_{pmdl}}, \tag{86}$$

where $K_{exact}^{cont} = -ik_x$ is the exact continuous half-space stiffness. Using (86), the stiffness of the PMDL layers can be written as

$$K_{pmdl} = \alpha K_{exact}^{cont}, \quad \text{where } \alpha = \frac{1 - R_n^{cont}}{1 + R_n^{cont}}. \tag{87}$$

Substituting (87) into (84), we get

$$R_n^{continuous\text{-}pmdl} = \frac{K_{exact}^{disc} - \alpha K_{exact}^{cont}}{K_{exact}^{disc} + \alpha K_{exact}^{cont}}. \tag{88}$$

Substituting the expressions for the half-space stiffnesses, (88) can be further simplified to

$$R_n^{continuous\text{-}pmdl} = \frac{\cos\left(\frac{kh}{2}\right) - \alpha}{\cos\left(\frac{kh}{2}\right) + \alpha}. \tag{89}$$

Thus (83) and (89) are the error measures when MD-PMDL and Continuous PMDL are used to approximate the right exterior and are plotted in Fig. 3. The reflection coefficients are plotted against normalized horizontal wavenumbers (kh) for a set of parameters (L_i's) that were chosen in an ad hoc fashion. The plot shows that at low wavenumbers the reflection coefficients are similar in magnitude for PMDL and MD-PMDL. However, for high wavenumbers MD-PMDL performs much better than PMDL which does not improve even with a large number of layers. This justifies our initial claim that continuum ABCs cannot be directly used to approximate discrete systems. We will now present some numerical results that shows the effectiveness of MD-PMDL.

5.3. Numerical experiment: 1-D discrete wave equation

The wave equation for a discrete half-space ($x \geqslant 0$) is given by

$$-D_x^2 u(x,t) + \frac{\partial^2 u(x,t)}{\partial t^2} = 0. \tag{90}$$

The domain of interest is chosen to be 10 atoms with positions $x_j = (j-1)h$, $j = 1, 2, \ldots, 10$, where h is the lattice spacing. The initial and the loading conditions are given by

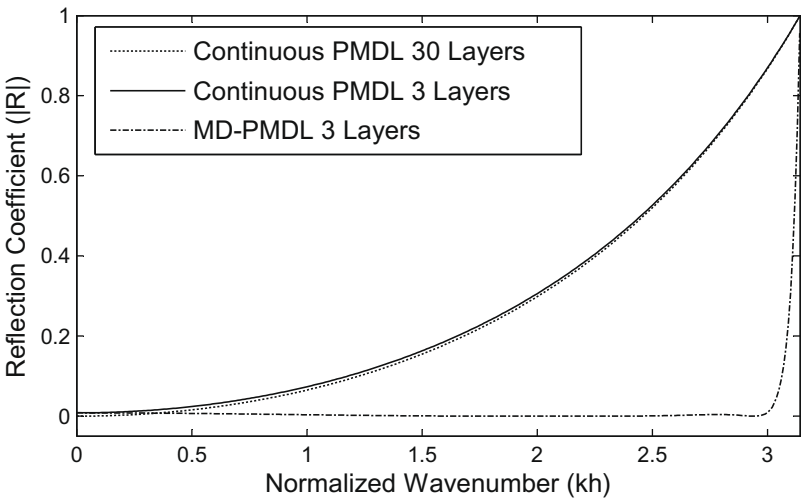

Fig. 3. Plot of the reflection coefficient when continuous PMDL and MD-PMDL boundary conditions are used for the discrete wave equation.

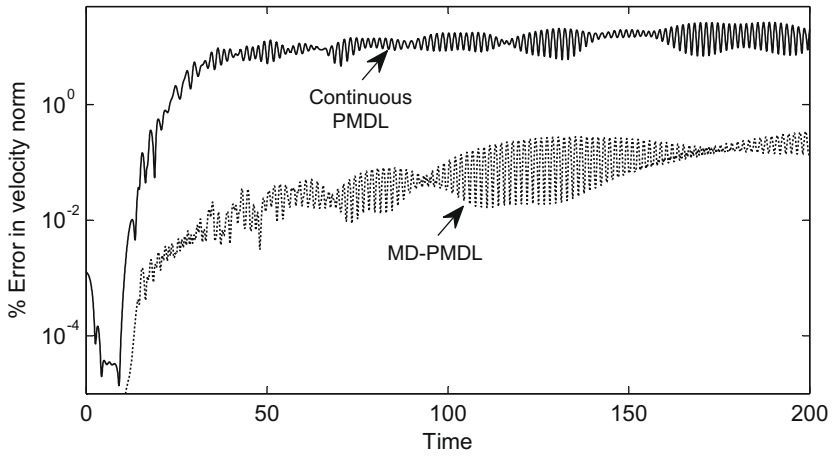

Fig. 4. A semilog plot of the evolution of relative error in velocity.

$$f(0,t) = \begin{cases} \sin^2\left(\frac{\pi}{2}t\right) & t < 2\pi \\ 0 & \text{otherwise} \end{cases}, \tag{91}$$

$$u(x,0) = 0, \tag{92}$$

$$\dot{u}(x,0) = 0. \tag{93}$$

The velocity norm is used as the criterion to compare the different boundary conditions, as it provides a measure of the total kinetic energy of the system and hence the temperature. The simulation is performed using MD-PMDL and continuous PMDL to approximate the discrete half-space. Three layers of MD-PMDL were used with parameters $\{(p_i,q_i) = (0,\frac{1}{16}), (0,\frac{4}{16}), (0,\frac{9}{16})\}$, and the same parameters are used for the PMDL boundary conditions. Note that the parameters were chosen in an ad hoc manner. The time evolution was performed using the velocity-verlet algorithm. The results are compared with the exact solution which is computed by using a much larger domain (1000 atoms) so that the boundary effects are not seen in the region of interest.

The relative errors from the two simulations are shown in Fig. 4. As expected, continuous PMDL has significant errors ($\sim 10\%$) while MD-PMDL has a much smaller error (0.2%).

6. MD-PMDL formulation for 2-D square lattice

A unit cell corresponding to a general 2-D square lattice can be written as

$$\underset{\substack{i=-\infty,\ldots,\infty \\ j=-\infty,\ldots,\infty}}{\mathbb{A}} \left\{ \begin{bmatrix} a_{11} & a_{12} & a_{13} & a_{14} \\ a_{21} & a_{22} & a_{23} & a_{24} \\ a_{31} & a_{32} & a_{33} & a_{34} \\ a_{41} & a_{42} & a_{43} & a_{44} \end{bmatrix} \right\} \mathbf{U} = \mathbf{F}, \tag{94}$$

which in turn can be expressed as

$$\underset{\substack{i=-\infty,\ldots,\infty \\ j=-\infty,\ldots,\infty}}{\mathbb{A}} \left\{ \begin{bmatrix} \begin{pmatrix} b_{11} & b_{12} \\ b_{21} & b_{11} \end{pmatrix} & \begin{pmatrix} b_{13} & b_{14} \\ b_{23} & b_{13} \end{pmatrix} \\ \begin{pmatrix} b_{31} & b_{32} \\ b_{41} & b_{31} \end{pmatrix} & \begin{pmatrix} b_{11} & b_{12} \\ b_{21} & b_{11} \end{pmatrix} \end{bmatrix} \right\} \mathbf{U} = \mathbf{F}, \tag{95}$$

where

$$\begin{aligned} b_{11} &= \frac{1}{4}(a_{11} + a_{22} + a_{33} + a_{44}), \\ b_{12} &= \frac{1}{2}(a_{12} + a_{34}), \quad b_{21} = \frac{1}{2}(a_{21} + a_{43}), \\ b_{13} &= \frac{1}{2}(a_{13} + a_{24}), \quad b_{31} = \frac{1}{2}(a_{31} + a_{42}), \\ b_{32} &= a_{32}, \quad b_{23} = a_{23}, \quad b_{41} = a_{41}, \quad b_{14} = a_{14}. \end{aligned}$$

Note that in (95), the operator on the left is of the form in (38) and hence can be expressed in terms of the basis matrices as

$$\mathop{\mathbb{A}}_{\substack{i=-\infty,\ldots,\infty\\ j=-\infty,\ldots,\infty}}\left\{\sum_{f\in\{-1,0,1\}}\mathbf{A}_f\otimes\mathbf{P}_f\right\}, \tag{96}$$

where

$$\begin{aligned}&\mathbf{P}_{-1}=\frac{\mathbf{P}}{2}-\frac{\mathbf{Q}+\mathbf{R}}{4},\quad \mathbf{P}_0=\frac{\mathbf{Q}-\mathbf{R}}{2},\quad \mathbf{P}_1=\frac{\mathbf{P}}{2}+\frac{\mathbf{Q}+\mathbf{R}}{4},\\ &\mathbf{P}=\begin{bmatrix}b_{11}&b_{12}\\ b_{21}&b_{11}\end{bmatrix},\quad \mathbf{Q}=\begin{bmatrix}b_{13}&b_{14}\\ b_{23}&b_{13}\end{bmatrix},\quad \mathbf{R}=\begin{bmatrix}b_{31}&b_{32}\\ b_{41}&b_{31}\end{bmatrix}\end{aligned} \tag{97}$$

Also, note that each of the matrices $\mathbf{P}$, $\mathbf{Q}$ and $\mathbf{R}$ can in turn be written in terms of the basis matrices. Thus we have

$$\mathbf{P}_f=\sum_{g\in\{-1,0,1\}}c_{f,g}\mathbf{A}_g, \tag{98}$$

and substituting (98) in (96), we get

$$\mathop{\mathbb{A}}_{\substack{i=-\infty,\ldots,\infty\\ j=-\infty,\ldots,\infty}}\left\{\sum_{f\in\{-1,0,1\}}\mathbf{A}_f\otimes\left(\sum_{g\in\{-1,0,1\}}c_{f,g}\mathbf{A}_g\right)\right\} \tag{99}$$

Thus, the governing equation for a general harmonic periodic square lattice can be written as

$$\mathop{\mathbb{A}}_{\substack{i=-\infty,\ldots,\infty\\ j=-\infty,\ldots,\infty}}\left\{\sum_{\substack{f\in\{-1,0,1\}\\ g\in\{-1,0,1\}}}c_{f,g}\mathbf{A}_f\otimes\mathbf{A}_g\right\}\mathbf{U}=\mathbf{F}, \tag{100}$$

where $c_{f,g}$ are constants that can be determined from the original system. We will now construct a PMDL lattice that has the same characteristic impedance as the system in (100) and hence the original harmonic system.

The 2-D assembly on the left hand side of (100) can be rewritten as a 1-D assembly

$$\mathop{\mathbb{A}}_{i=-\infty}^{\infty}\left\{\sum_{f\in\{-1,0,1\}}\mathbf{A}_f\otimes\mathbf{O}_f\right\}, \tag{101}$$

where

$$\mathbf{O}_f=\mathop{\mathbb{A}}_{j=-\infty}^{\infty}\left\{\sum_{g\in\{-1,0,1\}}c_{f,g}\mathbf{A}_g\right\}. \tag{102}$$

Note that the assembly in (101) is exactly the same as in (38), and hence can be rewritten (similar to the 1-D case) using (33) as

$$\mathop{\mathbb{A}}_{i=-\infty}^{\infty}\left\{\sum_{f\in\{-1,0,1\}}L_i^f\mathbf{A}_\mathbf{f}\otimes\mathbf{O}_f\right\}. \tag{103}$$

Substituting back $\mathbf{O}^\mathbf{f}$ from (102) into (103), we get

$$\mathop{\mathbb{A}}_{\substack{i=-\infty,\ldots,\infty\\ j=-\infty,\ldots,\infty}}\left\{\sum_{\substack{f\in\{-1,0,1\}\\ g\in\{-1,0,1\}}}c_{f,g}L_i^f\mathbf{A}_\mathbf{f}\otimes\mathbf{A}_\mathbf{g}\right\} \tag{104}$$

This procedure can be repeated in a similar fashion for the assembly along the y direction to get

$$\mathop{\mathbb{A}}_{\substack{i=-\infty,\ldots,\infty\\ j=-\infty,\ldots,\infty}}\left\{\sum_{\substack{f\in\{-1,0,1\}\\ g\in\{-1,0,1\}}}c_{f,g}L_i^fL_j^g\mathbf{A}_\mathbf{f}\otimes\mathbf{A}_\mathbf{g}\right\}. \tag{105}$$

The assembly in (105) is the final form of PMDL lattice that is equivalent (with respect to stiffness) to the original system and has exact stiffness matching property at any interface irrespective of the spacings L_i and L_j. Note that for the choice of $L_i = 1$ and $L_j = 1$, (105) is identical to the original matrix operator in (100).

Similar to the decomposition in the 1-D lattice, the 2-D lattice can also be split into an interior and an exterior system that are coupled by the boundary region, i.e.

$$\begin{aligned} \mathbf{A_{ii}U_i} &= \mathbf{F_i} - \mathbf{A_{ie}U_e}, \\ \mathbf{A_{ee}U_e} &= \mathbf{F_e} - \mathbf{A_{ei}U_i}. \end{aligned} \tag{106}$$

Since the interior is coupled with the exterior only along the boundary, and since the treatment of the interior is exactly the same as in the 1-D case, only the exterior needs to be discussed here. Note that the exterior can be viewed as an assembly of 3 super-cells $\mathbf{E_x}, \mathbf{E_y}$ and $\mathbf{C_{xy}}$ (see Fig. 5(b)), i.e.

$$\mathbf{A_{ee}U_e} = (\overline{\mathbf{P}} + \mathbb{A}\{\mathbf{E_x}, \mathbf{E_y}, \mathbf{C_{xy}}\})\mathbf{U_e}. \tag{107}$$

The super cells $\mathbf{E_x}$ and $\mathbf{E_y}$ will be referred to as edge exteriors as they extend to $+\infty$ along x and y, respectively. Similarly the super cell $\mathbf{C_{xy}}$ will be referred to as the corner exterior as it extends to $+\infty$ along both x and y directions. The system of equations for the super-cells is given by

$$\begin{aligned} \mathbf{E_x} &= \underset{\substack{i=1,\ldots,\infty \\ j=-\infty,\ldots,-1}}{\mathbb{A}} \left\{ \sum_{\substack{f\in\{-1,0,1\} \\ g\in\{-1,0,1\}}} c_{f,g} L_i^f \mathbf{A_f} \otimes \mathbf{A_g} \right\}, \\ \mathbf{E_y} &= \underset{\substack{i=-\infty,\ldots,-1 \\ j=1,\ldots,\infty}}{\mathbb{A}} \left\{ \sum_{\substack{f\in\{-1,0,1\} \\ g\in\{-1,0,1\}}} c_{f,g} L_j^g \mathbf{A_f} \otimes \mathbf{A_g} \right\}, \\ \mathbf{C_{xy}} &= \underset{\substack{i=1,\ldots,\infty \\ j=1,\ldots,\infty}}{\mathbb{A}} \left\{ \sum_{\substack{f\in\{-1,0,1\} \\ g\in\{-1,0,1\}}} c_{f,g} L_i^f L_j^g \mathbf{A_f} \otimes \mathbf{A_g} \right\}. \end{aligned} \tag{108}$$

We now need to truncate $\mathbf{E_x}$ along x and $\mathbf{E_y}$ along y and $\mathbf{C_{xy}}$ along both. Again, similar to the 1-D case, the truncated system can be written as

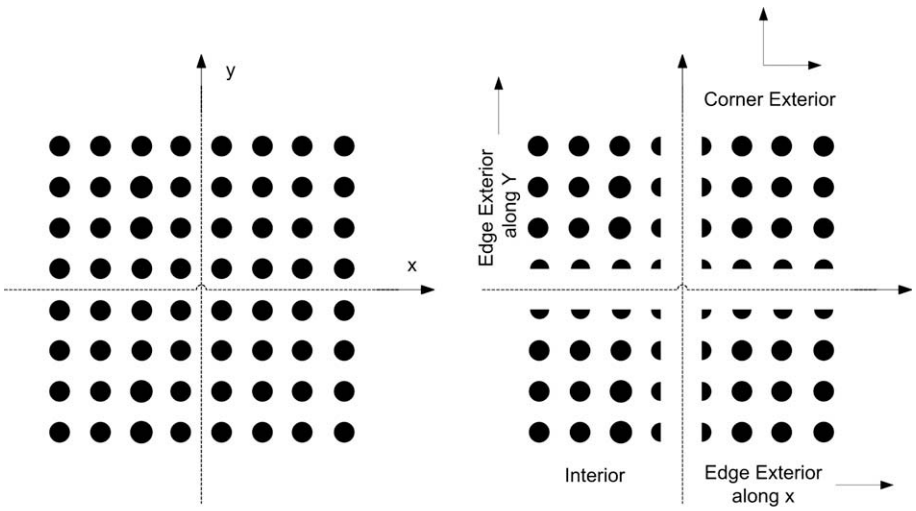

(a) A schematic of an infinite square lattice

(b) A schematic showing the defintion of Interior and Exteriors for a square lattice

Fig. 5. A schematic of an infinite square lattice.

$$\mathbf{E_x} = \underset{\substack{i=1,\ldots,m_x\\ j=-\infty,\ldots,-1}}{\mathbb{A}} \left\{ \sum_{\substack{f\in\{-1,0,1\}\\ g\in\{-1,0,1\}}} c_{f,g} L_i^f \mathbf{A_f} \otimes \mathbf{A_g} \right\},$$

$$\mathbf{E_y} = \underset{\substack{i=-\infty,\ldots,-1\\ j=1,\ldots,m_y}}{\mathbb{A}} \left\{ \sum_{\substack{f\in\{-1,0,1\}\\ g\in\{-1,0,1\}}} c_{f,g} L_j^g \mathbf{A_f} \otimes \mathbf{A_g} \right\}, \tag{109}$$

$$\mathbf{C_{xy}} = \underset{\substack{i=1,\ldots,m_x\\ j=1,\ldots,m_y}}{\mathbb{A}} \left\{ \sum_{\substack{f\in\{-1,0,1\}\\ g\in\{-1,0,1\}}} c_{f,g} L_i^f L_j^g \mathbf{A_f} \otimes \mathbf{A_g} \right\}$$

Note that the unit cell of $\mathbf{C_{xy}}$ reduces to that of $\mathbf{E_x}$ and $\mathbf{E_y}$ for $L_j = 1$ and $L_i = 1$, respectively. Thus, the formulation for $\mathbf{C_{xy}}$ is derived first and the formulations for $\mathbf{E_y}$ and $\mathbf{E_x}$ can then be obtained as a special case of the corner formulation.

6.1. Formulation for the corner exterior

The system of equations for the corner region $\mathbf{C_{xy}}$ is given by

$$\underset{\substack{i=1,\ldots,m_x\\ j=1,\ldots,m_y}}{\mathbb{A}} \left\{ \sum_{\substack{f\in\{-1,0,1\}\\ g\in\{-1,0,1\}}} c_{f,g} L_i^f L_j^g \mathbf{A_f} \otimes \mathbf{A_g} \right\} \mathbf{U_c} = \mathbf{F_c}. \tag{110}$$

Recall that the basis matrices can be decomposed as

$$\mathbf{A_{-1}} = \mathbf{v_{-1}} \mathbf{v_{-1}^t}, \quad \mathbf{A_0} = \mathbf{v_1} \mathbf{v_{-1}^t}, \quad \mathbf{A_1} = \mathbf{v_1} \mathbf{v_1^t}, \tag{111}$$

where $\mathbf{v_{-1}^t} = [-1\ 1]$ and $\mathbf{v_1^t} = [1\ 1]$. Based on (111), Kronecker product of any two basis matrices can be represented as

$$\mathbf{A_i} \otimes \mathbf{A_j} = (\mathbf{a_1} \mathbf{a_2^t}) \otimes (\mathbf{b_1} \mathbf{b_2^t}) = (\mathbf{a_1} \otimes \mathbf{b_1})(\mathbf{a_2} \otimes \mathbf{b_2})^{\mathbf{t}}. \tag{112}$$

Using (112) and (111), we can rewrite (110) as

$$\underset{\substack{i=1,\ldots,m_x\\ j=1,\ldots,m_y}}{\mathbb{A}} \left\{ \begin{array}{l} (\mathbf{v_{-1}} \otimes \mathbf{v_{-1}}) s_{1,(i,j)} + (\mathbf{v_{-1}} \otimes \mathbf{v_1}) s_{2,(i,j)} + \\ + (\mathbf{v_1} \otimes \mathbf{v_{-1}}) s_{3,(i,j)} + (\mathbf{v_1} \otimes \mathbf{v_1}) s_{4,(i,j)} + \\ + c_{0,0} (\mathbf{A_0} \otimes \mathbf{A_0}) \mathbf{u_{i,j}} \end{array} \right\} = \mathbf{F_c}, \tag{113}$$

where $\mathbf{s_1}, \mathbf{s_2}, \mathbf{s_3}$ and $\mathbf{s_4}$ are the state variables for the corner region and are given by

$$\begin{aligned} s_{1,(i,j)} &= \frac{c_{-1,-1}}{L_i L_j} (\mathbf{v_{-1}} \otimes \mathbf{v_{-1}})^{\mathbf{t}} \mathbf{u_{i,j}}, \\ s_{2,(i,j)} &= \frac{c_{-1,0}}{L_i} (\mathbf{v_{-1}} \otimes \mathbf{v_{-1}})^{\mathbf{t}} \mathbf{u_{i,j}} + \frac{c_{-1,1} L_j}{L_i} (\mathbf{v_{-1}} \otimes \mathbf{v_1})^{\mathbf{t}} \mathbf{u_{i,j}}, \\ s_{3,(i,j)} &= \frac{c_{0,-1}}{L_j} (\mathbf{v_{-1}} \otimes \mathbf{v_{-1}})^{\mathbf{t}} \mathbf{u_{i,j}} + \frac{c_{1,-1} L_i}{L_j} (\mathbf{v_1} \otimes \mathbf{v_{-1}})^{\mathbf{t}} \mathbf{u_{i,j}}, \\ s_{4,(i,j)} &= c_{0,1} L_j (\mathbf{v_{-1}} \otimes \mathbf{v_1})^{\mathbf{t}} \mathbf{u_{i,j}} + c_{1,0} L_i (\mathbf{v_1} \otimes \mathbf{v_{-1}})^{\mathbf{t}} \mathbf{u_{i,j}} + c_{1,1} L_i L_j (\mathbf{v_1} \otimes \mathbf{v_1})^{\mathbf{t}} \mathbf{u_{i,j}}. \end{aligned} \tag{114}$$

Once the state variables are defined, the derivation is identical to the 1-D derivation. Thus (114) is inverse Fourier transformed to obtain the time domain equations for the state variables which are then discretized using the Crank–Nicolson method to obtain the evolution equations for the state variables. These evolution equations are given by

$$\begin{aligned} s_{1,(i,j)}^{n+1} &= \frac{\hat{r}_i}{r_i} s_{1,(i,j)}^n + \frac{1}{r_i} \left(\hat{s}_{1,(i,j)}^{n+1} - \hat{s}_{1,(i,j)}^n \right), \\ \hat{s}_{1,(i,j)}^{n+1} &= \frac{\hat{r}_j}{r_j} \hat{s}_{1,(i,j)}^n + \frac{c_{-1,-1}}{r_j} (\mathbf{v_{-1}} \otimes \mathbf{v_{-1}})^{\mathbf{t}} \left(\mathbf{u_{i,j}^{n+1}} - \mathbf{u_{i,j}^n} \right), \end{aligned} \tag{115}$$

$$s_{2,(i,j)}^{n+1} = \frac{\hat{r}_i}{r_i} s_{2,(i,j)}^n + \frac{c_{-1,0}}{r_i} (\mathbf{v_{-1}} \otimes \mathbf{v_{-1}})^{\mathbf{t}} \left(\mathbf{u_{i,j}^{n+1}} - \mathbf{u_{i,j}^n} \right) + \frac{c_{-1,1}}{r_i} (\mathbf{v_{-1}} \otimes \mathbf{v_1})^{\mathbf{t}} \left(r_j \mathbf{u_{i,j}^{n+1}} - \hat{r}_j \mathbf{u_{i,j}^n} \right), \tag{116}$$

$$s_{3,(i,j)}^{n+1} = \frac{\hat{r}_j}{r_j} s_{3,(i,j)}^n + \frac{c_{0,-1}}{r_j} (\mathbf{v_{-1}} \otimes \mathbf{v_{-1}})^{\mathbf{t}} \left(\mathbf{u_{i,j}^{n+1}} - \mathbf{u_{i,j}^n} \right) + \frac{c_{1,-1}}{r_j} (\mathbf{v_1} \otimes \mathbf{v_{-1}})^{\mathbf{t}} \left(r_i \mathbf{u_{i,j}^{n+1}} - \hat{r}_i \mathbf{u_{i,j}^n} \right), \tag{117}$$

$$s^{n+1}_{4,(i,j)} = s^{n}_{4,(i,j)} + c_{0,1}(\mathbf{v}_{-1}\otimes\mathbf{v}_{1})^{\mathbf{t}}\left(r_j\mathbf{u}^{n+1}_{\mathbf{i,j}} - \hat{r}_j\mathbf{u}^{n}_{\mathbf{i,j}}\right) + c_{1,0}(\mathbf{v}_{1}\otimes\mathbf{v}_{-1})^{\mathbf{t}}\left(r_i\mathbf{u}^{n+1}_{\mathbf{i,j}} - \hat{r}_i\mathbf{u}^{n}_{\mathbf{i,j}}\right) + \left(r_i\hat{s}^{n+1}_{4,(i,j)} - \hat{r}_i\hat{s}^{n}_{4,(i,j)}\right),$$
$$\hat{s}^{n+1}_{4,(i,j)} = \hat{s}^{n}_{4,(i,j)} + c_{1,1}(\mathbf{v}_{1}\otimes\mathbf{v}_{1})^{\mathbf{t}}\left(r_j\mathbf{u}^{n+1}_{\mathbf{i,j}} - \hat{r}_j\mathbf{u}^{n}_{\mathbf{i,j}}\right). \tag{118}$$

Substituting (115)–(118) into (113) evaluated at $t = t_{n+1}$, we get the final system of equations for the corner exterior as

$$\mathbf{K}_{\mathbf{L},\mathbf{c_{xy}}}\mathbf{U}^{\mathbf{n+1}}_{\mathbf{c_{xy}}} = \mathbf{F}^{\mathbf{n+1}}_{\mathbf{c_{xy}}} - \mathbf{F}^{\mathbf{n}}_{\mathbf{sv},\mathbf{c_{xy}}} + \mathbf{K}_{\mathbf{R},\mathbf{c_{xy}}}\mathbf{U}^{\mathbf{n}}_{\mathbf{c_{xy}}}, \tag{119}$$

where $\mathbf{F}_{\mathbf{c_{xy}}}$ is the coupling force with the edge exteriors, $\mathbf{K}_{\mathbf{L},\mathbf{c_{xy}}}$ and $\mathbf{K}_{\mathbf{R},\mathbf{c_{xy}}}$ are the stiffness matrices and $\mathbf{F}_{\mathbf{sv},\mathbf{c_{xy}}}$ is the force term from the state variables. The explicit expressions for these are given by

$$\mathbf{K}_{\mathbf{L},\mathbf{c_{xy}}} = \underset{\substack{i=1,\ldots,m_x\\ j=1,\ldots,m_y}}{\mathbb{A}}\left\{\sum_{\substack{f\in\{-1,0,1\}\\ g\in\{-1,0,1\}}} c_{f,g}r_i^f r_j^g \mathbf{A}_{\mathbf{f}}\otimes\mathbf{A}_{\mathbf{g}}\right\}, \tag{120}$$

$$\mathbf{K}_{\mathbf{R},\mathbf{c_{xy}}} = \underset{\substack{i=1,\ldots,m_x\\ j=1,\ldots,m_y}}{\mathbb{A}}\left\{\begin{array}{l} \frac{c_{-1,-1}}{r_i r_j}\mathbf{A}_{-\mathbf{1}}\otimes\mathbf{A}_{-\mathbf{1}} + \frac{c_{-1,0}}{r_i}\mathbf{A}_{-\mathbf{1}}\otimes\mathbf{A}_{\mathbf{0}} + \\ \frac{\hat{r}_j c_{-1,1}}{r_i}\mathbf{A}_{-\mathbf{1}}\otimes\mathbf{A}_{\mathbf{1}} + \frac{c_{0,-1}}{r_j}\mathbf{A}_{\mathbf{0}}\otimes\mathbf{A}_{-\mathbf{1}} + \\ \hat{r}_j c_{0,1}\mathbf{A}_{\mathbf{0}}\otimes\mathbf{A}_{\mathbf{1}} + \frac{\hat{r}_i c_{1,-1}}{r_j}\mathbf{A}_{\mathbf{1}}\otimes\mathbf{A}_{-\mathbf{1}} + \\ \hat{r}_i c_{1,0}\mathbf{A}_{\mathbf{1}}\otimes\mathbf{A}_{\mathbf{0}} + r_i\hat{r}_j c_{1,1}\mathbf{A}_{\mathbf{1}}\otimes\mathbf{A}_{\mathbf{1}} \end{array}\right\}, \tag{121}$$

$$\mathbf{F}^{\mathbf{n}}_{\mathbf{sv},\mathbf{c_{xy}}} = \underset{\substack{i=1,\ldots,m_x\\ j=1,\ldots,m_y}}{\mathbb{A}}\left\{\begin{array}{l} \mathbf{v}_{-\mathbf{1}}\otimes\mathbf{v}_{-\mathbf{1}}\left[\frac{\hat{r}_i}{r_i}s^{n}_{1,(i,j)} + \frac{\hat{r}_j}{r_i r_j}\hat{s}^{n}_{1,(i,j)}\right] + \\ +\mathbf{v}_{-\mathbf{1}}\otimes\mathbf{v}_{\mathbf{1}}\frac{\hat{r}_i}{r_i}s^{n}_{2,(i,j)} + \mathbf{v}_{\mathbf{1}}\otimes\mathbf{v}_{-\mathbf{1}}\frac{\hat{r}_j}{r_j}s^{n}_{3,(i,j)} + \\ +\mathbf{v}_{\mathbf{1}}\otimes\mathbf{v}_{\mathbf{1}}[s^{n}_{4,(i,j)} + (r_i - \hat{r}_i)\hat{s}^{n}_{4,(i,j)}] \end{array}\right\}. \tag{122}$$

6.2. Formulation for edge exteriors

The state variables for the edge exterior along $x(\mathbf{E_x})$ can be obtained from (114) by setting $L_j = 1$ and are given by

$$\begin{aligned} s_{1,(i,j)} &= \frac{c_{-1,-1}}{L_i}(\mathbf{v}_{-\mathbf{1}}\otimes\mathbf{v}_{-\mathbf{1}})^{\mathbf{t}}\mathbf{u}_{\mathbf{i,j}},\\ s_{2,(i,j)} &= \frac{c_{-1,0}}{L_i}(\mathbf{v}_{-\mathbf{1}}\otimes\mathbf{v}_{-\mathbf{1}})^{\mathbf{t}}\mathbf{u}_{\mathbf{i,j}} + \frac{c_{-1,1}}{L_i}(\mathbf{v}_{-\mathbf{1}}\otimes\mathbf{v}_{\mathbf{1}})^{\mathbf{t}}\mathbf{u}_{\mathbf{i,j}},\\ s_{3,(i,j)} &= c_{1,-1}L_i(\mathbf{v}_{\mathbf{1}}\otimes\mathbf{v}_{-\mathbf{1}})^{\mathbf{t}}\mathbf{u}_{\mathbf{i,j}},\\ s_{4,(i,j)} &= c_{1,0}L_i(\mathbf{v}_{\mathbf{1}}\otimes\mathbf{v}_{-\mathbf{1}})^{\mathbf{t}}\mathbf{u}_{\mathbf{i,j}} + c_{1,1}L_i(\mathbf{v}_{\mathbf{1}}\otimes\mathbf{v}_{\mathbf{1}})^{\mathbf{t}}\mathbf{u}_{\mathbf{i,j}}. \end{aligned} \tag{123}$$

Substituting L_i in (123) and following the same procedure as for the corner, we get the evolution equations for the state variables as

$$s^{n+1}_{1,(i,j)} = \frac{\hat{r}_i}{r_i}s^{n}_{1,(i,j)} + \frac{c_{-1,-1}}{r_i}(\mathbf{v}_{-\mathbf{1}}\otimes\mathbf{v}_{-\mathbf{1}})^{\mathbf{t}}\left(\mathbf{u}^{n+1}_{\mathbf{i,j}} - \mathbf{u}^{n}_{\mathbf{i,j}}\right), \tag{124}$$

$$s^{n+1}_{2,(i,j)} = \frac{\hat{r}_i}{r_i}s^{n}_{2,(i,j)} + \frac{c_{-1,0}}{r_i}(\mathbf{v}_{-\mathbf{1}}\otimes\mathbf{v}_{-\mathbf{1}})^{\mathbf{t}}(\mathbf{u}^{n+1}_{\mathbf{i,j}} - \mathbf{u}^{n}_{\mathbf{i,j}}) + \frac{c_{-1,1}}{r_i}(\mathbf{v}_{-\mathbf{1}}\otimes\mathbf{v}_{\mathbf{1}})^{\mathbf{t}}(\mathbf{u}^{n+1}_{\mathbf{i,j}} - \mathbf{u}^{n}_{\mathbf{i,j}}), \tag{125}$$

$$s^{n+1}_{3,(i,j)} = s^{n}_{3,(i,j)} + c_{1,-1}(\mathbf{v}_{\mathbf{1}}\otimes\mathbf{v}_{-\mathbf{1}})^{\mathbf{t}}(r_i\mathbf{u}^{n+1}_{\mathbf{i,j}} - \hat{r}_i\mathbf{u}^{n}_{\mathbf{i,j}}), \tag{126}$$

$$s^{n+1}_{4,(i,j)} = s^{n}_{4,(i,j)} + c_{1,0}(\mathbf{v}_{\mathbf{1}}\otimes\mathbf{v}_{-\mathbf{1}})^{\mathbf{t}}(r_i\mathbf{u}^{n+1}_{\mathbf{i,j}} - \hat{r}_i\mathbf{u}^{n}_{\mathbf{i,j}}) + c_{1,1}(\mathbf{v}_{\mathbf{1}}\otimes\mathbf{v}_{\mathbf{1}})^{\mathbf{t}}(r_i\mathbf{u}^{n+1}_{\mathbf{i,j}} - \hat{r}_i\mathbf{u}^{n}_{\mathbf{i,j}}). \tag{127}$$

The stiffness matrices and the state variable force are given by

$$\mathbf{K}_{\mathbf{L},\mathbf{e_x}} = \underset{\substack{i=1,\ldots,m_x\\ j=-\infty,\ldots,-1}}{\mathbb{A}}\left\{\sum_{\substack{f\in\{-1,0,1\}\\ g\in\{-1,0,1\}}} c_{f,g}r_i^f \mathbf{A}_{\mathbf{f}}\otimes\mathbf{A}_{\mathbf{g}}\right\} \tag{128}$$

$$\mathbf{K}_{\mathbf{R},\mathbf{e_x}} = \underset{\substack{i=1,\ldots,m_x\\ j=-\infty,\ldots,-1}}{\mathbb{A}}\left\{\begin{array}{l} \frac{c_{-1,-1}}{r_i}\mathbf{A}_{-\mathbf{1}}\otimes\mathbf{A}_{-\mathbf{1}} + \frac{c_{-1,0}}{r_i}\mathbf{A}_{-\mathbf{1}}\otimes\mathbf{A}_{\mathbf{0}} + \\ \frac{c_{-1,1}}{r_i}\mathbf{A}_{-\mathbf{1}}\otimes\mathbf{A}_{\mathbf{1}} + \hat{r}_i c_{1,-1}\mathbf{A}_{\mathbf{1}}\otimes\mathbf{A}_{-\mathbf{1}} + \\ \hat{r}_i c_{1,0}\mathbf{A}_{\mathbf{1}}\otimes\mathbf{A}_{\mathbf{0}} + \hat{r}_i c_{1,1}\mathbf{A}_{\mathbf{1}}\otimes\mathbf{A}_{\mathbf{1}} \end{array}\right\}, \tag{129}$$

$$\mathbf{F}^{\mathbf{n}}_{\mathbf{sv},\mathbf{e_x}} = \underset{\substack{i=1,\ldots,m_x\\ j=-\infty,\ldots,-1}}{\mathbb{A}}\left\{\begin{array}{l} \mathbf{v}_{-\mathbf{1}}\otimes\mathbf{v}_{-\mathbf{1}}\frac{\hat{r}_i}{r_i}s^{n}_{1,(i,j)} + \mathbf{v}_{-\mathbf{1}}\otimes\mathbf{v}_{\mathbf{1}}\frac{\hat{r}_i}{r_i}s^{n}_{2,(i,j)} + \\ +\mathbf{v}_{\mathbf{1}}\otimes\mathbf{v}_{-\mathbf{1}}s^{n}_{3,(i,j)} + \mathbf{v}_{\mathbf{1}}\otimes\mathbf{v}_{\mathbf{1}}s^{n}_{4,(i,j)}. \end{array}\right\}. \tag{130}$$

A similar procedure can be followed to get the contributions from the edge exterior along y. Thus, the combined system of equations for the exterior can be written as

$$\mathbf{K_L U_e^{n+1}} = \mathbf{F_e^{n+1}} - \mathbf{F_{sv}^n} + \mathbf{K_R U_e^n}, \tag{131}$$

where

$$\mathbf{K_L} = \mathbb{A}\{\mathbf{K_{L,c_{xy}}}, \mathbf{K_{L,e_y}}, \mathbf{K_{L,e_x}}\} + \overline{\mathbf{P}}, \tag{132}$$

$$\mathbf{K_R} = \mathbb{A}\{\mathbf{K_{R,c_{xy}}}, \mathbf{K_{R,e_y}}, \mathbf{K_{R,e_x}}\}, \tag{133}$$

$$\mathbf{F_{sv}^n} = \mathbb{A}\left\{\mathbf{F_{sv,c_{xy}}^n}, \mathbf{F_{sv,e_x}^n}, \mathbf{F_{sv,e_y}^n}\right\}. \tag{134}$$

Remark on computational cost: Note that the formulations in (131) and (54) are implicit, as the atoms in the PMDL exterior are coupled. This is in contrast with explicit computations in the interior and raises the issue of computational overhead due to MD-PMDL. Fortunately, the cost of these implicit computations are not significant due to the local nature of the coupling in MD-PMDL. Note that the left-hand-side operator in (131) is local in space, thus indicating sparse matrices and linear scaling of computational cost associated with factorization. Furthermore, assuming constant time increment, such factorization needs to be performed only once at the beginning of analysis and the cost of solving sparse triangular matrices is similar to explicit computation. Thus, the additional overhead due to MD-PMDL is not very significant.

Generalization to complex lattice systems: While the development of MD-PMDL is limited to simple square lattice systems in this paper, the methodology presented here is quite general and a formal extension to more complex lattice systems is straightforward. The basic idea is that a complex lattice can be viewed as a square lattice but with multiple atoms associated with each lattice site. In other words the unit cell for a complex lattice is identical to (94) but the matrix elements are in turn block matrices. Following the same procedure, i.e. (95)–(105), to obtain the equivalent discrete lattice, we get a similar form

$$\mathop{\mathbb{A}}_{\substack{i=-\infty,\ldots,\infty\\ j=-\infty,\ldots,\infty}} \left\{ \sum_{\substack{f\in\{-1,0,1\}\\ g\in\{-1,0,1\}}} L_i^f L_j^g \mathbf{C}_{f,g} \otimes \mathbf{A_f} \otimes \mathbf{A_g} \right\}, \tag{135}$$

where $\mathbf{C}_{f,g}$ are block matrices as compared to constants in (105). While the procedure is straightforward, the stability properties for this extension are not very clear. Complex lattice systems contain optical branches in their dispersion relation where the group and phase velocities may have opposite signs. Such a situation necessitates careful choice of PMDL parameters to avoid instabilities [18,22]. Extension of MD-PMDL for complex lattice systems and resolution of associated stability issues are subjects of future research and will be reported in future publications.

6.3. Numerical experiment: 2-D discrete wave equation

The wave equation for a discrete half-space in 2-D ($x \geqslant 0 \cup y \geqslant 0$) is given by

$$-D_x^2 u - D_y^2 u + \frac{\partial^2 u}{\partial t^2} = f. \tag{136}$$

The domain of interest has 100 atoms along each dimension and the external force is applied at the node at position (75,75) of the square lattice. The domain of interest here is taken larger than the 1-D problem so that the wave reflections can be seen clearly at the edges. The simulation is performed using both MD-PMDL and continuous PMDL boundary conditions

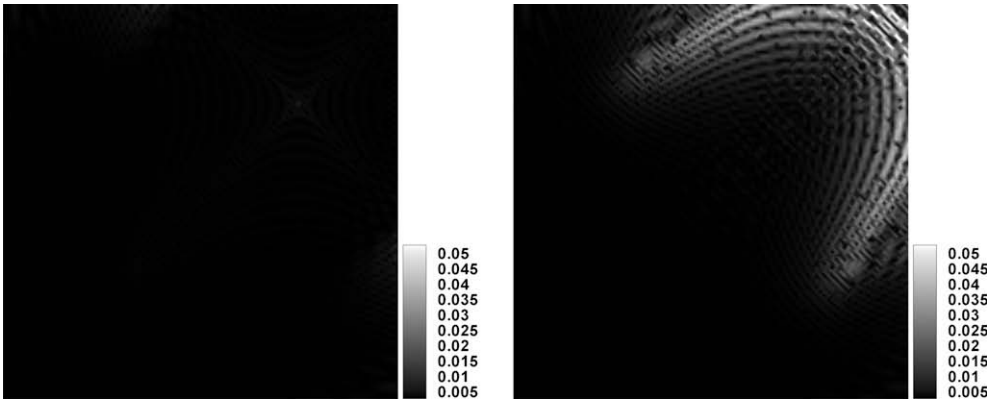

Fig. 6. The reflected energy contours at $t = 100$ for the 2-D discrete wave equation using (a) MD-PMDL and (b) continuous PMDL boundary conditions.

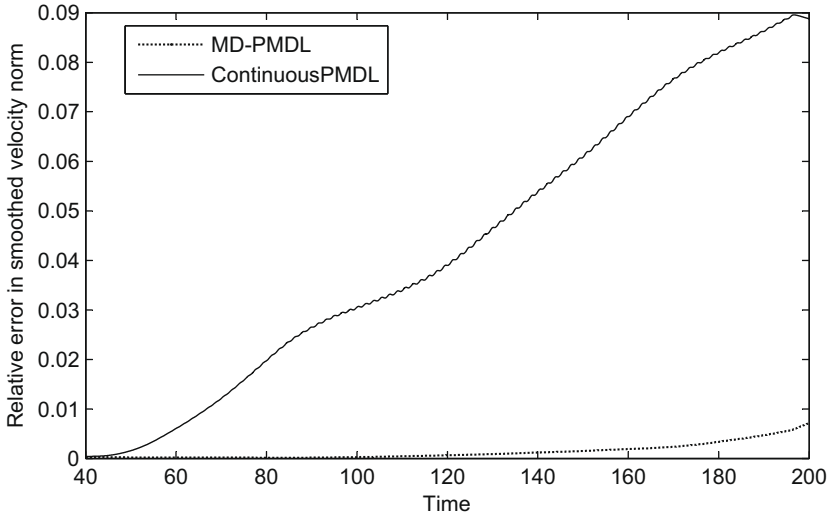

Fig. 7. Plot of the evolution of relative error in velocity norm.

Fig. 8. A schematic of the setup for crack simulation.

and compared with the exact solution that is obtained by simulating a much larger domain. The loading and initial conditions are given by

$$f(75,75,t) = \begin{cases} 10 * \sin(0.9 * \pi t)^2 & t < 100\left(\frac{\pi}{0.9}\right) \\ 0 & \text{otherwise} \end{cases}, \tag{137}$$

$$u(i,j,0) = 0, \tag{138}$$

$$\dot{u}(i,j,0) = 0. \tag{139}$$

The parameters for both PMDL and MD-PMDL are taken as $\{(p_i, q_i) = (0,1)\}$ and velocity-verlet algorithm is used for the time-stepping. Fig. 6 shows the energy contours at $t = 100$. The figure clearly shows significant reflection at the corner boundary for continuous PMDL as compared to hardly any reflections for MD-PMDL boundary conditions. Also, Fig. 7 shows the error evolution over the duration of the simulation and again the superior absorption properties of MD-PMDL are clearly seen (MD-PMDL has an error of <1% while continuous PMDL's error reaches 9%). Based on the 1-D and 2-D results, we can conclude that MD-PMDL is more accurate in phonon absorption than continuous PMDL.

6.4. Numerical experiment: mode 3 fracture

In this simulation, a semi-infinite strip with an initial crack is subjected to out-of-plane displacements resulting in a steady growth of the initial crack. The aim of the simulation is to see the effectiveness of MD-PMDL in absorbing the phonons emitted due to the breaking of bonds during crack propagation. While this is not a full fledged crack propagation simulation, it gives an idea of the usefulness of MD-PMDL in a realistic fracture simulation involving moving boundaries (which is out of scope of this paper). This example also illustrates the applicability of MD-PMDL where the interior is nonlinear.

We used the Slepyan model of fracture in which the atoms are connected to the neighbors through bonds that are elastic when the deformation is less than a limit, $u_f = 2$, and snap when the deformation exceeds the limit. The same setup as in [23] was used to study the effect of the high frequency phonons that are emitted when the bonds break. The setup is as shown in Fig. 8. The interior is a rectangular grid that is 20 atoms wide and 100 atoms long. The initial crack is taken to be 20 atoms long.

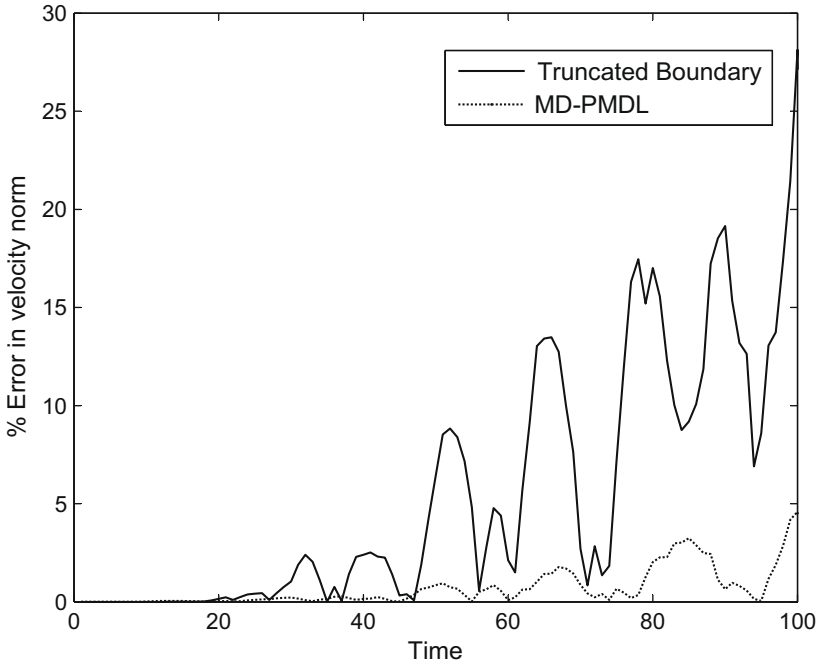

Fig. 9. Plot of the relative error in velocity norm in a small region (40 atoms wide) near the left boundary.

The exterior region is approximated using MD-PMDL using 5 identical layers with parameters $\{(p_i, q_i) = (0, 1)\}$. The other boundary condition used for comparison is a buffer region that is 10 atoms wide with a Dirichlet condition at the end. Also, Dirichlet conditions $u = +U$ and $-U$ are applied at the top and bottom row of atoms. The Dirichlet condition at the left edge is taken to be $+U$ for atoms above the crack and $-U$ for the atoms below the crack, and for the right edge is taken to vary linearly from $-U$ at the bottom row to $+U$ at the top row. Also, for the atoms outside the initial cracked zone, the initial displacements are taken to vary linearly between the Dirichlet conditions at the top and bottom rows. For the atoms in the cracked zone, the initial conditions are taken to vary linearly between the Dirichlet condition at the left edge and the initial displacement immediately to the right of the crack tip. The value of U is taken to be 20 for this simulation. The initial velocities are taken to be zero over the entire domain.

In [23], the authors use moving boundaries to simulate a steady state crack growth. However, steady state growth is not simulated in this example and the crack is allowed to grow from initial configuration until it reaches the end of the domain. The velocity norm is measured for a small region (40 atoms wide) near the left boundary to see the effect of reflections due to phonons. The simulations are carried out for MD-PMDL and a truncated boundary with an offset of 10 atoms. The results are compared against the exact solution obtained using a much larger domain. Fig. 9 shows the error in velocity norm and it is clear that MD-PMDL performs better than a truncated boundary (MD-PMDL has <5% error while truncated BC has almost 30% error). Though the magnitude of the values are small, this would be significant in an actual fracture simulation with moving boundaries as the domain size would be small and reflection of phonons back into the domain will pose a major problem. This example also demonstrates that MD-PMDL performs well for the case of nonlinear interaction in the interior domain.

7. Concluding remarks

We have presented a systematic procedure to develop ABCs for MD domains and have demonstrated through numerical examples that they are superior in performance compared to their continuum counterparts. This validates our initial assertion that a continuous ABC cannot be used directly for the MD domain.

We also presented an explicit expression for the error estimate in terms of the parameters of the boundary condition. The error estimate makes the approximation characteristics of the boundary condition transparent, indicating that it can be easily optimized for performance.

The final form of the boundary conditions for 1-D and 2-D lattices is presented in an explicit form that is easy to implement. We note that while the boundary condition couples the domain along the boundary, it is still local to the region near the boundary. Since the error decays exponentially with the number of layers, often only a few layers are needed to obtain accurate results. Thus, the additional overhead due to MD-PMDL is not high. Also, the method does not involve any expensive convolution operations as it is *completely* local in time. The only computational burden is the solution of sparse linear system (factorization needs to be done just once). While explicit comparison with other existing MD-ABCs is not made, we believe that the local nature of MD-PMDL provides an efficient alternative to existing MD-ABCs.

While MD-PMDL's effectiveness was illustrated for a square lattice with scalar field variable, the derivation of MD-PMDL is applicable for a vector equation. Thus, it should be possible to extend MD-PMDL for more complex lattices by expressing them as a simple lattice with multiple degrees of freedom per node. However, complex lattices involve optical phonon branches that are similar to dispersion branches for elastic wave propagation in continuous waveguides. Since PMDL has stability issues in simulating elastic waves in layers [18], we anticipate that the extension to complex lattices might not be straightforward and would be investigated in the future.

The current formulation is limited to the case of zero temperature in the exterior. For a more realistic simulation, MD-PMDL should be extended to handle non-zero temperatures in the exterior (heat bath). This extension to non-zero temperature would be investigated in the near future; we intend to build on the existing ideas in treating heat bath (see [15]).

Another area of focus is the extension of MD-PMDL as an interface condition for atomistic-continuum coupling (see [13,24,25]). While interface conditions act like an ABC in dissipating the high frequency phonons, they also need to enable the exchange of information with the continuum domain. A related extension would be for moving boundaries for simulating processes such as dynamic crack propagation and moving dislocation.

Acknowledgments

This work originated from MNG's sabbatical leave at the Program in Applied and Computational Mathematics in Princeton University. He thanks Weinan E for his hospitality and for several insightful discussions on this topic. This work also benefited from discussions with Phani Nukala, Xiantao Li and Siddharth Savadatti. The authors thank Mehran Eslaminia for carefully checking the manuscript.

References

[1] D. Givoli, Non-reflecting boundary conditions: a review, J. Comput. Phys. 94 (1991) 1–29.
[2] X. Antoine, A. Arnold, C. Besse, M. Ehrhardt, A. Schädle, A review of transparent and artificial boundary conditions techniques for linear and nonlinear schrödinger equations, Commun. Comput. Phys. 4 (2008) 729–796.
[3] S. Adelman, J. Doll, Generalized langevin equation approach for atom/solid-surface scattering: general formulation for classical scattering off harmonic solids, J. Chem. Phys. 64 (1976) 2375.
[4] W. Cai, M.D. Konin, V.V. Bulatov, S. Yip, Minimizing boundary reflections in coupled-domain simulations, Phys. Rev. Lett. 85 (2000) 3213–3216.
[5] E.G. Karpov, G.J. Wagner, W.K. Liu, A green's function approach to deriving non-reflecting boundary conditions in molecular dynamics simulations, Int. J. Numer. Meth. Eng. 62 (9) (2005) 1250–1262.
[6] H.S. Park, E.G. Karpov, W.K. Liu, Non-reflecting boundary conditions for atomistic, continuum and coupled atomistic/continuum simulations, Int. J. Numer. Meth. Eng. 64 (2005) 237–259.
[7] P.C.Y.S. Namilae, D.M. Nicholson, D.J. Keffer, Absorbing boundary conditions for molecular dynamics and multiscale modeling, Phys. Rev. B 76 (14) (2007) 144111.
[8] J.P. Bérenger, A perfectly matched layer for the absorption of electromagnetic waves, J. Comput. Phys. 114 (1994) 185–200.
[9] T. Hagstrom, New results on absorbing layers and radiation boundary conditions, in: M. Ainsworth (Ed.), Topics in Computational Wave Propagation, Springer, New York, 2003, pp. 1–42.
[10] S. Li, X. Liu, A. Agrawal, A.C. To, Perfectly matched multiscale simulations for discrete systems: extension to multiple dimensions, Phys. Rev. B 74 (2006) 045418.
[11] W.C. Chew, W.H. Weedon, A 3-d perfectly matched medium from modified maxwells equations with stretched coordinates, Microwave Opt. Technol. Lett. 7 (1994) 599–604.
[12] M. Guddati, X. Li, An analysis of domain truncation techniques for molecular dynamics simulation, in preparation.
[13] X. Li, W. E, Variational boundary conditions for molecular dynamics simulations of solids at low temperature, Commun. Comput. Phys. 1 (2006) 136–176.
[14] W. E, Z. Huang, Matching conditions in atomistic-continuum modeling of material, Phys. Rev. Lett. 87 (2001) 135501.
[15] X. Li, W. E, Variational boundary conditions for molecular dynamics simulations of crystalline solids at finite temperature: treatment of the thermal bath, Phys. Rev. B 76 (10) (2007) 104107.
[16] B. Engquist, A. Majda, Radiation boundary conditions for acoustic and elastic wave calculations, Commun. Pure Appl. Math. 32 (3) (1979) 313–357.
[17] M.N. Guddati, K.W. Lim, Continued fraction absorbing boundary conditions for convex polygonal domains, Int. J. Numer. Meth. Eng. 66 (2006) 949–977.
[18] M. Guddati, K. Lim, M. Zahid, Perfectly matched discrete layers for unbounded domain modeling, in: E.F. Mogoules (Ed.), Computational Methods for Acoustics Problems, Saxe-Coburg, London, 2007, pp. 1–42.
[19] L. Brillouin, Wave Propagation in Periodic Structures: Electric Filters and Crystal Lattices, Dover, 1953.
[20] T. Hughes, The Finite Element Method, Dover, 2000.
[21] M.N. Guddati, Arbitrarily wide-angle wave equations for complex media, Comput. Meth. Appl. Mech. Eng. 195 (2006) 65–93.
[22] E. Bécache, S. Fauqueux, P. Joly, Stability of perfectly matched layers, group velocities and anisotropic waves, J. Comput. Phys. 188 (2) (2003) 399–433.
[23] M. Marder, S. Gross, Origin of crack tip instabilities, J. Mech. Phys. Solids 43 (1995) 1–48.
[24] W.K. Liu, H.S. Park, D. Qian, E.G. Karpov, H. Kadowaki, G.J. Wagner, Bridging scale methods for nanomechanics and materials, Comput. Meth. Appl. Mech. Eng. 195 (13-16) (2006) 1407–1421.
[25] S.P. Xiao, T. Belytschko, A bridging domain method for coupling continua with molecular dynamics, Comput. Meth. Appl. Mech. Eng. 193 (2004) 1645–1669.